AD-A185 424 HIGH PEAK POWER KA-BAND GYROTRON OSCILLATOR EXPERIMENT (U) NAVAL RESEARCH LAB WASHINGTON DC S H GOLD ET AL. 21 SEP 87 NRL-MR-5923 1/1

UNCLASSIFIED F/G 9/1 NL

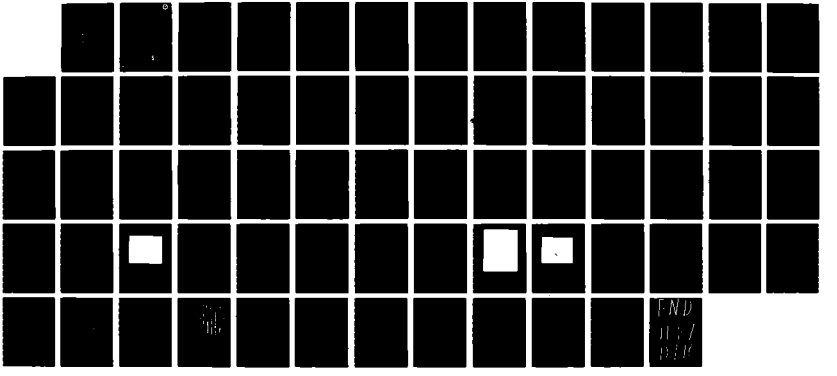

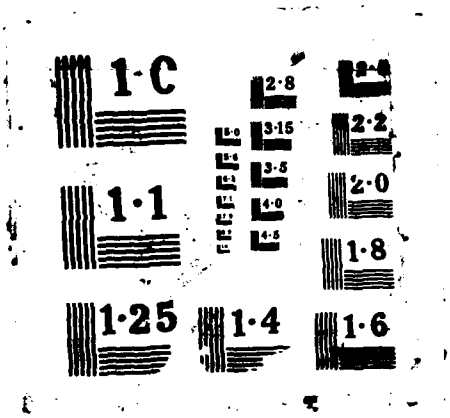
1·C
1·1
1·25
1·4
2·8
3·15
3·5
4·0
4·5
2·2
2·0
1·8
1·6

**Naval Research Laboratory**
Washington, DC 20375-5000

NRL Memorandum Report 5923



# High Peak Power $K_a$-Band Gyrotron Oscillator Experiment

S. H. GOLD, A. W. FLIFLET, W. M. MANHEIMER, R. B. MCCOWAN,*
W. M. BLACK, R. C. LEE,† V. L. GRANATSTEIN,‡
A. K. KINKEAD, D. L. HARDESTY, AND M. SUCY†

*High Power Electromagnetic Radiation Branch*
*Plasma Physics Division*

**Science Applications International Corporation*
*McLean, VA 22102*

†*JAYCOR, Inc.*
*Vienna, VA 22180*

‡*University of Maryland*
*College Park, MD 20742*

September 21, 1987

A185 424

SECURITY CLASSIFICATION OF THIS PAGE

# REPORT DOCUMENTATION PAGE

| | |
|---|---|
| 1a. REPORT SECURITY CLASSIFICATION<br>UNCLASSIFIED | 1b. RESTRICTIVE MARKINGS |
| 2a. SECURITY CLASSIFICATION AUTHORITY | 3. DISTRIBUTION / AVAILABILITY OF REPORT<br>Approved for public release; distribution unlimited. |
| 2b. DECLASSIFICATION / DOWNGRADING SCHEDULE | |
| 4. PERFORMING ORGANIZATION REPORT NUMBER(S)<br>NRL Memorandum Report 5923 | 5. MONITORING ORGANIZATION REPORT NUMBER(S) |
| 6a. NAME OF PERFORMING ORGANIZATION<br>Naval Research Laboratory<br>6b. OFFICE SYMBOL (If applicable)<br>Code 4740 | 7a. NAME OF MONITORING ORGANIZATION |
| 6c. ADDRESS (City, State, and ZIP Code)<br>Washington, DC 20375-5000<br>(See page ii) | 7b. ADDRESS (City, State, and ZIP Code) |
| 8a. NAME OF FUNDING / SPONSORING ORGANIZATION<br>(See page ii)<br>8b. OFFICE SYMBOL (If applicable) | 9. PROCUREMENT INSTRUMENT IDENTIFICATION NUMBER |
| 8c. ADDRESS (City, State, and ZIP Code)<br>(a) Arlington, VA 22217<br>(b) Washington, DC 20301-7100 | 10. SOURCE OF FUNDING NUMBERS<br>PROGRAM ELEMENT NO. (See page ii) / PROJECT NO. / TASK NO. (See page ii) / WORK UNIT ACCESSION NO. (See page ii) |
| 11. TITLE (Include Security Classification) | |
| 12. PERSONAL AUTHOR(S) Gold, S.H., Fliflet, A.W., Manheimer, W.M., McCowan*, R.B., Black, W.M., Lee,† R.C., Granatstein,‡ V.L., Kinkead, A.K., Hardesty, D.L. and Sucy,† M. | |
| 13a. TYPE OF REPORT<br>Interim<br>13b. TIME COVERED<br>FROM 3/85 TO 3/86 | 14. DATE OF REPORT (Year, Month, Day)<br>1987 September 21<br>15. PAGE COUNT<br>66 |
| 16. SUPPLEMENTARY NOTATION *Science Applications Internation Corp., McLean, VA 22102<br>†JAYCOR, Inc., Vienna, VA 22180 ‡University of Maryland, College Park, MD 20742 | |

| 17. COSATI CODES | | |
|---|---|---|
| FIELD | GROUP | SUB-GROUP |
| | | |
| | | |

18. SUBJECT TERMS (Continue on reverse if necessary and identify by block number)
$K_a$-band gyrotron oscillator; Azimuthal index; Pulseline accelerator; Guide magnetic field; Frequency tuning

19. ABSTRACT (Continue on reverse if necessary and identify by block number)

A $K_a$-band gyrotron oscillator powered by a 600 kV pulseline accelerator has produced approximately 100 kW at 35 GHz in a circular $TE_{62}$ mode. It has also demonstrated frequency tuning over the range 28 to 49 GHz by operating in a family of $TE_{m2}$ modes, with the azimuthal index $m$ ranging from 4 to 10, by variation of the guide magnetic field. Operation is in general agreement with the predictions of theory.

| | |
|---|---|
| 20. DISTRIBUTION / AVAILABILITY OF ABSTRACT<br>X UNCLASSIFIED/UNLIMITED ☐ SAME AS RPT. ☐ DTIC USERS | 21. ABSTRACT SECURITY CLASSIFICATION<br>UNCLASSIFIED |
| 22a. NAME OF RESPONSIBLE INDIVIDUAL<br>Steven H. Gold | 22b. TELEPHONE (Include Area Code)<br>(202) 767-3358<br>22c. OFFICE SYMBOL<br>Code 4740 |

DD FORM 1473, 84 MAR 83 APR edition may be used until exhausted. All other editions are obsolete.

SECURITY CLASSIFICATION OF THIS PAGE
UNCLASSIFIED

10. SOURCE OF FUNDING NUMBERS

| PROGRAM ELEMENT NO. | PROJECT NO. | TASK NO. | WORK UNIT ACCESSION NO. |
|---|---|---|---|
| 61153N<br>RDT&EA | | RR011-09-41<br>HDL 264629 | DN880-061<br>DN156-218 |

CONTENTS




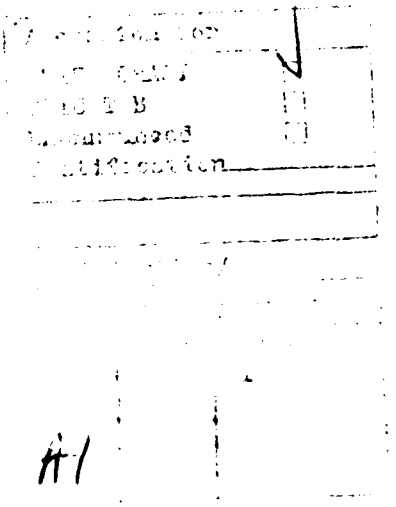

# HIGH PEAK POWER $K_a$ GYROTRON OSCILLATOR EXPERIMENT

## I. Introduction

Gyrotron oscillators employing thermionic cathode technology have proved to be highly efficient, exceptionally high average power millimeter-wave sources.[1] Operating at moderate currents and voltages (typically, $\lesssim$50 A at $\lesssim$100 keV), they have demonstrated 100s of kW of average power at efficiencies approaching 50%.[2] However, some future applications of millimeter-wave radiation, such as radars and very high energy electron linear accelerators,[3] may require substantially higher peak power levels than have been demonstrated using these conventional thermionic microwave tube technologies. This will require the application of much higher beam powers, requiring the use of both higher currents and voltages. In light of these general considerations, a research program was initiated to investigate the potential of gyrotron oscillators driven by the substantially higher currents and voltages available for short pulses ($\lesssim$100 nsec) from high voltage pulseline accelerators driving plasma-induced field emission cathodes.

Studies of the gyrotron interaction using pulseline accelerators have been in progress for more than a decade. Among the initial studies was one using a 3.3 MeV pulser to demonstrate microwave peak powers of approximately 1 GW at a frequency of 8 GHz in the $TE^{o}_{01}$ mode;[4] however, no resonant cavity was employed, and the superradiant device produced microwaves with an efficiency of less than 1%. Subsequent studies employing resonant cavities were carried out primarily in the Soviet Union, often employing accelerating voltages of approximately 350 kV and operating in a $TE^{o}_{1n}$ mode of a gyrotron cavity. Results of these studies included the demonstration of 23 MW at 40 GHz with 5% efficiency.[5]

Manuscript approved December 4, 1986.

Studies of pulseline driven millimeter-wave gyrotrons are also in progress in the United Kingdom.[6]

Our own recent studes have centered on "whispering-gallery" mode gyrotrons (i.e., $TE^{o}_{mn}$ modes with m>>n) which have good features for very high peak power generation of millimeter waves. The whispering-gallery gyrotrons interact preferentially with annular electron beams of large radius, and have superior mode stability without the aid of slots in the cavity walls. Thermionic cathode gyrotrons employing whispering gallery modes have the best performance for long pulse tubes at frequencies above 100 GHz. Among the results are output powers of 120 kW at 375 GHz and 15% efficiency for a pulse duration of 100 μsec,[7] and 645 kW at 140 GHz at 19% efficiency, with a peak efficiency of 24% at 300 kW for a pulse duration of 3 μsec.[8] These devices have the potential for further development to achieve cw operation.

In a previous paper,[9] we reported the production of 20 nsec pulses with 20 MW peak power at 35 GHz and 8% efficiency in a $TE_{62}$ mode from a gyrotron oscillator operating at approximately 350 kV and employing currents in the range of 0.5 to 1 kA. That earlier result was produced by an experiment operating on a 600 kV Febetron pulser capable of providing 6 kA of current into a matched 100 Ω load. However, the previous experiment was constrained to lower currents and voltages by limitations inherent in its diode design. In this paper, we report further experiments in which the Febetron pulser was operated at its full voltage of 600 kV, and mismatched upwards at the diode to produce a peak diode voltage approaching 800 kV at a diode current of ~3.5 kA. These experiments were carried out employing a similar microwave circuit to that reported in the earlier work, but using an improved method of forming the 1-3 kA high

transverse momentum beam required for gyrotron operation. As a result of these improvements, the output power was increased to approximately 100 MW at 35 GHz in a $TE_{62}$ mode with an efficiency of approximately 8%. In addition, by tuning the cavity magnetic field while keeping the beam parameters fixed, it was possible to demonstrate the operation of the experiment at high power in a sequence of $TE_{m2}$ modes, with the azimuthal index m ranging from 4 to 10, while tuning the operating frequency over the range of 28 to 49 GHz.

A detailed comparison of the experimental data with theory shows interesting features for gyrotron operation with high voltage electron beams. Rapid changes in cyclotron frequency due to electron mass variation with beam voltage allows operation in the "hard excitation" regime[10] with a pulsed device. This effect also appears to enhance the stability of single mode operation.

## II. Experimental Setup

Figure 1 illustrates the experimental setup. A 600 kV compact Febetron pulser with 100 Ω impedance and 55 nsec output voltage pulse is used to generate an electron beam in a simple foilless diode geometry, in which the anode is simply the outer metallic cylinder enclosing the diode region. The electrons are emitted from the sharpened edge of a 3.44-cm-diam. cylindrical carbon cathode by means of explosive plasma formation. The diode is immersed in the field of the main solenoidal magnet. The impedance of this diode is determined by the limiting current for the electron beam as it streams away from the cathode along the guide magnetic field. In this case, a beam of approximately 3.5 kA is produced.

Additional transverse momentum is induced by sending the beam past a "pump" magnet which produces a localized dip in the axial magnetic field. During adiabatic changes in the axial magnetic field, the ratio $p_t^2/B$ remains constant, where $p_t$ is the transverse component of the electron momentum and B is the magnetic field; however, the non-adiabatic change in the axial magnetic field produced by the "pump" magnet increases the magnetic moment of the electron trajectories. Typically, an approximate 50% magnetic field reduction at the center of the dip at the initial radius of the electron beam is required in order to produce a significant non-adiabatic effect on the transverse electron momentum. After emerging from the region of the dip, the electron beam transverse momentum is further increased as the beam is adiabatically compressed to its final radius and magnetic field by the additional fields provided by the cavity solenoid. Each of the three magnets is powered by a separate capacitor bank discharge, to allow separate adjustment of the electron transverse momentum, the magnetic field compression ratio, and the final magnetic field.

Fig. 2 illustrates typical experimental waveforms for the diode voltage and current, the net gyrotron current measured by the Rogowski coil, and a typical microwave signal measured by a crystal detector. The FWHM of the diode voltage pulse is ~55 nsec. However, it lacks a true "flat-top", or period of constant voltage, and has two separate voltage maxima separated by ~30 nsec, with the first peak about 25% higher than the second. Operating conditions are typically selected to maximize the 35 GHz microwave emission in the vicinity of the first voltage maximum. In this case, the microwave signal will typically have a total width of approximately 20 nsec, as illustrated in Fig. 2, which corresponds to

operation during a time when the diode voltage undergoes a 20-25% rise and fall. The implications of this time-dependent voltage waveform will be discussed further below.

The combination of the "pump" magnet and the subsequent adiabatic compression can result in the experimental loss of a portion of the electron beam current prior to the gyrotron cavity. This is due to the increase in transverse velocity (and consequent decrease in streaming velocity) as the beam is magnetically compressed, combined with the effect of space charge depression of the beam kinetic energy, due to the separation of the electron beam from the conducting wall. For any combination of fields at the cathode and in the cavity, the optimum operating point of the experiment is selected by varying the "pump" magnet amplitude in order to maximize the microwave signal that is synchronous with the maximum of the voltage waveform. This optimum was always found to correspond to a "pump" magnet amplitude that substantially reduced the current streaming through the gyrotron cavity, as determined by the Rogowski coil. (See Fig. 1.) Typically, the microwave optimum was found to correspond to a condition in which half or less of the initial beam current reached the gyrotron cavity. Such a case is illustrated in Fig. 2. The remaining current is assumed to reflect back towards the diode during the adiabatic compression, and is most likely collected on the drift tube wall at the magnetic field minimum in the vicinity of the "pump" magnet.

For these experiments, a cavity radius of 1.6 cm was selected, in order to place the operating frequency for a gyrotron in the $TE_{62}$ mode at approximately 35 GHz. The cavity is fabricated from stainless steel, to facilitate the penetration of pulsed magnetic fields, and is coated with

gold to reduce ohmic losses. Its input end has a tapered section, extending to below cutoff of the desired operating modes, in order to taper the axial profile of the microwave electromagnetic fields for reasons of efficiency enhancement. The output end of the cavity is defined by a change in wall slope from 0° to 5°. The 5° output taper extends outward to the 7-cm radius of the output waveguide. The output waveguide ends in a 14-cm-diam. vacuum window. The length of the cavity corresponds to approximately 6-8 cyclotron orbits for a 600 keV electron beam with $\alpha$-1, where $\alpha$ is the ratio of transverse to axial electron velocity, and the cavity quality factor Q is -250. The frequencies of the lowest axial wavenumber (i.e. $\ell$=1) $TE_{mn\ell}$ and $TM_{mn\ell}$ modes in the vicinity of 35 GHz are shown in Fig. 3.

## III. Experimental Results

### A. Microwave measurements

The microwave measurement system consists of two separate detection channels. Each channel is composed entirely of "in-band" WR-28 components and begins with a small microwave aperture antenna positioned within 1 cm of the output window of the experiment. The apertures that are employed for this purpose are the open ends of sections of WR-28 waveguide. Each aperture is connected via a section of flexible waveguide to -11 m of rigid waveguide leading to a screen room, and can be positioned independently at any position on the output window to detect either radial or azimuthal polarization. The entire output window, except for the location of the apertures, is covered with microwave absorber to eliminate stray reflections. In the screen room, each signal is attenuated by

transit through the coupled port of a 20 dB directional coupler, and by a calibrated rotary-vane attenuator. The signals are further processed either by a low pass filter, that strongly attenuates out-of-band signals above 40 GHz, or by a combination of a low pass filter and a narrow-band (1.6 GHz FWHM) step-twist filter[11] that limits the transmitted signal to a narrow frequency range about 35 GHz. (The WR-28 waveguide itself serves as a high pass filter, with a cutoff frequency of 21.2 GHz.) Finally, the microwave signals are detected by $K_a$-band crystal detectors, which have been calibrated throughout their operating range against a thermistor power meter.

It was observed via open shutter photography (see Fig. 4) that the microwave electric fields were causing air breakdown streamers to form on the ends of the apertures and to extend upstream from the antenna to the output window. In order to eliminate this effect, which could interfere with the detection of the microwave signal, and still permit near-field measurements of the output mode pattern, a microwave-attenuating window was placed at the end of the experiment in place of the highly transmissive polyethylene vacuum window that is customarily employed. This "lossy" window consists of nominal 1-inch-thick (~2.5 cm) phenolic plastic, which produces a signal attenuation of 10±0.5 dB, as calibrated by measuring the normal incidence free-space attenuation at 35 GHz between two standard $K_a$-band horns. With the power density reduced by an order of magnitude by this means, no further streamer formation was observed on the microwave apertures.

Figure 5 shows a typical microwave scan of the operating mode, with the Febetron operating at its full erected voltage of 600 kV, and driving a diode impedance that is mismatched upward by approximately a factor of

2, to produce a peak diode voltage of ~775 kV. The average gyrotron current at the first voltage maximum for this data set is ~1.6 kA, slightly less than half of the total diode current of ~3.5 kA. The electron beam radius in the gyrotron cavity is ~1.2 cm, or ~0.75 of the cavity wall radius. Assuming a beam $\alpha$~1, the calculated space-charge depression of the beam is ~40 keV. The magnetic field in the cavity is $B_o$=23.8 kG. This data was taken with one microwave aperture (Channel #2) kept at a fixed location on the output window as a monitor of shot-to-shot reproducibility, and the second detection channel (#1) used to scan the output mode on a shot-to-shot basis as a function of radius and electric-field polarization across a single radius of the output window. Typically, three shots were taken at each position, and an average value calculated over the three measured values of detected power. This measured mode pattern can be compared to the predictions for the three TE modes available to the interaction near 35 GHz, as illustrated in Fig. 6. Note that the power measured in the radial pattern in $E_r$ compared to that in $E_\theta$ may be somewhat affected by the presence of an azimuthal standing wave, as discussed below. Note also, for purposes of comparison with Fig. 6, that the measurement is made just beyond a 2.54-cm-thick output window, and that the mode will begin to diverge after leaving the output waveguide. There is no evidence for the excitation of the $TE_{14}$ mode, whose principal maximum is on axis. Similarly, there is no evidence of the excitation of the $TE_{10,1}$ mode, which is a true whispering-gallery mode and should have large radial maxima in $|E_r|^2$ and $|E_\theta|^2$ adjacent to the edge of the output waveguide. The match is best to the $TE_{62}$-mode (as also observed in the earlier experiment[9]). This is consistent with Fig. 7, which indicates that the normalized beam radius of ~0.75 is close to

optimum for coupling to the $TE_{-6,2}$ mode, where the minus sign is defined with reference to the sense of the axial magnetic field in the cavity, and indicates that the mode is rotating opposite to the sense of electron gyration. However, the match is not perfect, and there is some evidence that the mode observed at the output window may no longer be the pure $TE_{62}$ mode that should be produced in the cavity. This lack of a pure $TE_{62}$ mode may be due in part to mode conversion, either in the 5° uptaper that begins at the end of the cavity, or due to imperfections in the 1.6-m length of the 14-cm-diam. output waveguide. (The 5° uptaper replaced a 10° uptaper used in the previous experiment,[9] in order to reduce mode conversion effects.)

The measured mode pattern can also be used to estimate the peak power. This is done by integrating the measured mode pattern across the face of the output window, and absolutely calibrating the detection system. To proceed, we first average the detected power across the measured mode pattern in radial and azimuthal polarizations. The results are 0.61 mW and 0.71 mW, respectively. Next, it is necessary to account for the following loss factors: 1) the ratio of the effective aperture of the microwave antenna to the area of the of the mode (29.07 dB, based on a measured mode radius of 7.25 cm and an effective aperture for the antenna that is 81% of its physical aperture),[12] 2) window attenuation (10±.5 dB), 3) measured waveguide loss between the aperture and the directional coupler (11.35 dB), 4) signal reduction due to a directional coupler (20.75 dB), 5) the setting on a calibrated rotary-vane attenuator (36 dB), and 6) filter and miscellaneous loss factors in the waveguide connecting to the crystal detectors (1.02 dB). The values given in parentheses correspond to the loss factors for detection channel #1 for

the data of Fig. 5, and their sum is 108.19 dB. The average power seen at the detector, summed over polarization, is 1.32 mW. Multiplying this value by the measured and calculated loss factors produces a power estimate of 87 MW. This corresponds to an approximate efficiency of 7%, based on a peak voltage of ~775 kV, and neglecting the effects of space-charge depression and the time-dependent voltage waveform. This estimate is produced by an averaging process over many shots; based on the scatter in the data points, the best single shot power is estimated to be somewhat (~1 dB) higher, or approximately 110 MW (~9% efficiency). The overall uncertainty of this power determination, based on error bars in the averaging process and in the various multiplicative factors, is estimated to be ±2.2 dB.

One complication in the averaging process is the presence of an azimuthal standing-wave component in the microwave mode pattern, due to the excitation of both the $TE_{+62}$ and $TE_{-62}$ circularly-polarized cavity modes. The observation of such structures is discussed in the following section on breakdown studies, and there is some evidence that the azimuthal phase of the standing component is not completely random on a shot-to-shot basis. Since only a single radius is scanned in Fig. 5, such a standing structure, if not corrected for, could bias the power estimate. However, for the data presented in Fig. 5, this is not believed to cause a substantial bias to the power calculation for the following reasons: 1) The azimuthal variation observed in a scan at the radial maxima is only ±1 dB (i.e., the output mode is predominantly a rotating mode, due to the location of the beam at a minimum for coupling to the $TE_{+62}$ mode), and 2) Since $|E_r|^2$ and $|E_\theta|^2$ each contain about half of the total power, and they are spatially out of phase around the azimuth, any

bias in favor of one component of the rf electric field would be compensated by a bias against the orthogonal component. The effect of azimuthal asymmetry is included in the overall error estimate.

Figure 8 shows a plot of output power at 35 GHz at the first voltage maximum versus cavity magnetic field for constant current, voltage, and normalized beam radius in the gyrotron cavity. The output power is approximately flat from 23 to 24.5 kG. It falls off abruptly to zero when the magnetic field is decreased from 23 kG to 22.5, but decreases gradually to zero as the magnetic field is increased from 24.5 kG to 26 kG. This tuning range is consistent with the broad interaction bandwidth predicted for the relatively short cavity employed in these experiments, but it is also believed to be related to the mode density of the cavity and the time-dependent voltage waveform. This is discussed further in Section V.

B. Breakdown studies

The use of microwave-induced gas breakdown as a diagnostic of the operating mode of the gyrotron was discussed in an earlier paper.[9] Here we note simply that the addition of a low pressure cell (see Fig. 9) enclosing the output window of the gyrotron permits the selection of a suitable ambient pressure at which microwave-induced gas breakdown will occur across the face of the output window. Variation of the ambient pressure allows the adjustment of the electric field threshold for the breakdown process. Such variation could in principle allow a contour map of the output mode pattern to be built up over successive shots, but in practice, limitations in the shot-to-shot reproducibility, as well as the lack of a complete theory for the breakdown process in the vicinity of the

window surface, makes this difficult. Nevertheless, the pressure may be chosen to suppress breakdown at local minima, and permit breakdown at local maximum of the microwave electric field distribution. Observation of such breakdowns via open-shutter photography permits a global view of the microwave emission on a single-shot basis, which is a valuable supplement to the local measurements that are possible using small apertures feeding microwave crystal detectors, and assists in mode identification. Furthermore, the observation of an azimuthal standing structure in a particular discharge makes possible an unambiguous determination of the azimuthal index "m" of an operating $TE_{mn}$ or $TM_{mn}$ mode, which, combined with a knowledge of the magnetic field in the cavity, permits a straightforward determination of the operating mode and therefore of the approximate frequency of operation.

Figures 10 and 11 contain two end-on open shutter photographs of microwave-induced gas breakdown that were produced during a sequence of experimental discharges at fixed beam compression ratio and approximately constant current and voltage during which the axial magnetic field in the cavity was progressively decreased from an initial value of ~31kG. The normalized beam radius in the cavity for this data set was ~0.67, or ~1.07 cm, with a total beam thickness of ~4-6 mm, including both Larmor motion and guiding center spread. These photographs indicate the excitation of a pair of modes at 30.3 and 28.7 kG with azimuthal indices of 10 to 9 and similar radial structure. Additional photographs at progressively lower magnetic fields indicate that this sequence can be extended through a sequence of $TE_{mn}$ or $TM_{mn}$ modes with similar radial structure down to an azimuthal index of 4, which was observed at a cavity magnetic field of 16.3 kG. (The azimuthal structure is progressively more difficult to see

as m drops below 6, indicating that the emission becomes more circularly polarized at lower magnetic fields.) Reference to a mode map for the gyrotron cavity clearly indicates that this set of photographs depicts a sequence of $TE_{m2}$ modes, with m ranging from 4 to 10, and corresponding to frequencies ranging from 28 to 49 GHz. Reference to Fig. 7 illustrates that this is a favorable radius for excitation of both the $TE_{+62}$ and $TE_{-62}$ modes, and this will remain approximately true for most of the other $TE_{\pm m2}$ modes, as well. (Note that the normalized beam radius of 0.75 for the microwave data of Fig. 5 is at the coupling maximum for the $TE_{-62}$ mode and at a zero for the coupling to the $TE_{+62}$ mode: the apparent standing structure for such cases is much weaker.) Separate microwave power determinations were not performed for the various modes observed in this sequence. However, based on the relative brightness of the discharges at a constant ambient pressure of ~100 Torr in the breakdown chamber, it appears that the power generally increases with frequency over this mode sequence.

The result of the mode scan is illustrated in Fig. 12, which plots each of the observed $TE_{m2}$ modes against the magnetic field at which it was most pronounced in a breakdown picture, and against the predicted frequency of the mode at cutoff in the gyrotron cavity. The "best fit" straight line passing through the origin is illustrated in the figure. This line corresponds to exact cyclotron resonance for ~390 keV. By contrast, the peak electron kinetic energy is ~720 keV, assuming a peak voltage of 775 kV in the diode, and ~55 kV of beam space charge depression in the cavity. Alternatively, this line would correspond to the formula $f=1.37\Omega_o/2\pi\gamma_{eff}$, where $\Omega_o$ is the nonrelativistic cyclotron frequency in the cavity magnetic field, and the relativistic factor $\gamma_{eff}=2.41$ is

calculated for the peak electron kinetic energy of 720 keV. This would correspond to an effective detuning $[1-\Omega_o/\gamma_{eff}\omega]$ of the gyrotron interaction of -27% from exact resonance. The theoretically predicted optimum detuning is -15%. The reason for this apparent large detuning is believed to be the highly time-dependent nature of the voltage waveform, as discussed in Section V. Assuming that the "best fit" line corresponds to the center of a tuning range for excitation of each of the modes, a "stair-step" function is superimposed over this line, corresponding to the approximate range over which each mode should be tunable. Each of the experimental points appears to fall on one of the steps of this function.

By varying the beam radius in the cavity, additional modes can be excited, as indicated by the observation of completely different radial structures in the breakdown image, but their precise identification is more ambiguous due to lack of clear azimuthal structure. To date, there has been no unambiguous evidence for the excitation of modes with m=1, such as the $TE_{14}$ mode that is nearly degenerate in frequency with the $TE_{62}$ mode. This fact is consistent with the higher starting current predicted for $TE_{1n}$ modes, compared to the whispering-gallery modes, for large beam radii.

## IV. Theory

The theory of high voltage gyrotron operation closely parallels that for lower voltage devices, except for the increased coupling that is possible to TM modes of the gyrotron cavity. A discussion of some of the design considerations for high voltage gyrotrons is given in Ref. 13. The

theory of gyrotron oscillators has received considerable attention.[14-21] The theory used in the design and interpretation of the present experiment is summarized below.

The self-consistent field equations for the gyrotron in steady-state operation can be written in the following compact form:[16,21]

$$\frac{dp}{d\zeta} = -\frac{1}{2} p^{s-1} \mathrm{Re}\{F\, e^{-i\theta}\} \tag{1a}$$

$$\frac{d\theta}{d\zeta} = \Delta - 1 + p^2 + \frac{s}{2} p^{s-2} \mathrm{Re}\{iF\, e^{-i\theta}\} \tag{1b}$$

$$\left(\frac{d^2}{d\zeta^2} + \delta\right)F = iI\langle p^s e^{i\theta}\rangle_{\theta_o} \tag{1c}$$

where p and $\theta$ are slow-time-scale transverse momentum amplitude and phase variables for a beam electron, $\zeta$ is the axial coordinate, s is the harmonic number, F is the waveguide mode transverse field amplitude, $\Delta$ is the interaction detuning parameter, I is the beam current parameter, and $\delta$ is proportional to the square of the local axial wavenumber. These normalized parameters are defined as follows:

$$p = \frac{p_t}{\gamma_o m_o c \beta_{to}} \tag{2a}$$

$$\zeta = \frac{\beta_{to}^2 \omega z}{2\beta_{zo} c} \tag{2b}$$

$$\Delta = \frac{2}{\beta_{to}^2}\left(1 - \frac{s\Omega}{\omega}\right) \tag{2c}$$

$$\delta = \frac{8\beta_{zo}}{\beta_{to}^4} \frac{\omega - \omega_{co}}{\omega} \tag{2d}$$

where $p_t$ is the unnormalized momentum amplitude, $\gamma_o$ is the relativistic mass ratio prior to the interaction, $m_o$ is the electron rest mass, c is the speed of light, $\beta_{to}$ and $\beta_{zo}$ are the initial transverse and axial velocities normalized to the speed of light, $\omega$ is the wave frequency, $\omega_{co}$ is the local cut-off frequency of the operating mode, and $\Omega$ is the initial relativistic cyclotron frequency given by

$$\Omega = \frac{|e|B_o}{m_o\gamma_o} \quad . \tag{3}$$

Here e is the electron charge and $B_o$ is the applied (axial) magnetic field. $\langle \rangle_{\theta_o}$ denotes an average with respect to the initial electron phase which in a free-running oscillator is uniformly distributed. All formulae are given in MKS units except as noted. For the case of a thin annular electron beam interacting in a circular cross section cavity with circularly polarized radiation having azimuthal dependence $\exp[i(m\theta-\omega t)]$, the field amplitude and current parameter for a $TE_{mn}$ mode are given by:

$$F = \frac{4|e|\beta_{to}^{s-4}C_{mn}J_{m-s}(k_{mn}r_b)}{\gamma_o m_o c^2}\,\frac{s^s}{2^s s!}\,f \tag{4a}$$

$$I = \frac{32\mu_o|e|I_o\beta_{zo}}{m_o c\gamma_o\beta_{to}^6}\,C_{mn}^2J_{m-s}^2(k_{mn}r_b)\left\{\frac{s^2}{2^s s!}\,\beta_{to}^{s-1}\right\}^2 \tag{4b}$$

and for a TM mode are given by:

$$F = \frac{4|e|}{\gamma_o m_o c} \beta_{to}^{s-4} \beta_{zo} C_{mn} J_{m-s}(k_{mn} r_b) \frac{s^s}{2^s s!} g \tag{5a}$$

$$I = \frac{32 \mu_o |e| I_o \beta_{zo}^3}{\gamma_o m_o \omega \beta_{to}^6} C_{mn}^2 J_{m-s}^2(k_{mn} r_b) \{\frac{s^s}{2^s s!} \beta_{to}^{s-1}\}^2 \tag{5b}$$

where f is the equivalent voltage amplitude of the transverse electric field, g is the equivalent current amplitude of the transverse magnetic field (see Ref. 22), $r_b$ is the beam radius in the cavity, $\mu_o = 4\pi \times 10^{-7}$ H/m is the permeability of free space, $I_o$ is the dc beam current, $J_{m-s}$ is a Bessel function and

$$C_{mn} = ([\pi(x'^2_{mn} - m^2)]^{1/2} J_m(x'_{mn}))^{-1} \tag{6a}$$

$$k_{mn} = \frac{x'_{mn}}{r_w} \tag{6b}$$

for a TE mode, or

$$C_{mn} = [\pi^{1/2} x_{mn} J'_m(x_{mn})]^{-1} \tag{7a}$$

$$k_{mn} = \frac{x_{mn}}{r_w} \tag{7b}$$

for a TM mode, where $x'_{mn}$ is the nth zero of $dJ_m(x)/dx$, $x_{mn}$ is the nth zero of $J_m(x)$, and $r_w$ is the radius of the gyrotron cavity.

In the self-consistent field (SCF) model, the axial variation of the cavity rf fields is determined self-consistently with the electron beam motion by integrating the wave equation [Eq. (1c)] simultaneously with the electron equations of motion.[21] The model accounts for important aspects

of gyrotron motion such as modification of the cavity Q and resonant frequency by beam loading. The steady-state characteristics of a gyrotron oscillator are obtained by integrating Eqs. (1) subject to appropriate initial conditions on the beam electrons and the rf field, and imposing an outgoing wave boundary condition on the rf field at the cavity output. For a cold beam, the initial conditions on the electrons are: $p_j(0)=1$, $\theta_j(0)=2\pi j/n$, $j=1,\ldots,N$. The rf field usually has the form of a growing evanescent wave at the cavity input and can be specified by an amplitude and a frequency. For a phase-mixed electron beam, the initial rf field phase is arbitrary. The output boundary condition for the rf field is given by

$$\left.\frac{dF}{d\zeta}\right|_{\zeta=\zeta_f} = ik_\zeta F(\zeta_f) \tag{8}$$

where $k_\zeta$ is the axial wavenumber in the output guide. Since F is complex, Eq. (8) represents two conditions. Thus the solution of Eqs. (1) constitutes a two parameter eigenvalue problem. For fixed beam, magnetic field, and cavity parameters, the eigenfunctions correspond to discrete pairs of values for $F(\zeta_o)$ and $\omega$. These are not known a priori and must be found by a search procedure.

To carry out gyrotron optimization and scaling studies, it is desirable to replace the self-consistent model by a simpler theory. This can be obtained by neglecting beam loading effects so that the axial as well as the transverse rf field structure is determined by the cavity (i.e., the cold cavity approximation). In this case, Eq. (1c) is eliminated and a fixed axial profile function for the rf field is introduced of the form

$$F(\zeta) = F_o h(\zeta) \tag{9}$$

where $F_o$ is the peak field amplitude and $h(\zeta)$ is the profile function with peak amplitude of unity. Convenient functional forms for $h(\zeta)$ include the Gaussian:

$$h(\zeta) = \exp[-\sigma(\frac{2\zeta}{\mu} - 1)^2] \tag{10}$$

where $\mu$ is the normalized interaction length, and $\sigma$ is an adjustable parameter; and the sinusoidal:

$$h(\zeta) = \sin(\ell\pi\zeta/\mu) \tag{11}$$

where $\ell$ is the longitudinal mode index. The Gaussian profile gives more accurate efficiency estimates, while the sinusoidal profile is more convenient for analytical studies.

For a given harmonic and choice of profile function, and optimizing with respect to the detuning parameter $\Delta$, the transverse efficiency depends only on $F_o$ and $\mu$ and is given by

$$\eta_t = 1 - \langle p(F_o, \mu) \rangle_{\theta_o} \tag{12}$$

The electronic efficiency is related to the transverse efficiency according to:

$$\eta = \frac{\beta_{to}^2}{2(1-\gamma_o^{-1})}\,\eta_t \qquad (13)$$

Assuming a Gaussian profile function with $\sigma=2$, the output power is given by

$$P = \frac{\pi}{32}\left(\frac{\pi}{2\sigma}\right)^{1/2}\frac{c^3 m_o^2}{\mu_o e^2}\left(\frac{2^s s!}{s^s}\right)^2\frac{(x'^2_{mn}-m^2)}{J^2_{m-s}(k_{mn}r_b)}J^2_m(x'_{mn})\,\frac{\beta_{zo}\beta_{to}^{6-2s}\gamma_o^2\mu F^2}{Q} \qquad (14)$$

for a TE mode and by

$$P = \frac{\pi}{32}\left(\frac{\pi}{2\sigma}\right)^{1/2}\frac{c^3 m_o^2}{\mu_o e^2}\left(\frac{2^s s!}{s_s}\right)^2\frac{x^2_{mn}J'^2_m(x_{mn})}{J^2_{m-s}(k_{mn}r_b)}\,\frac{\beta_{to}^{6-2s}}{\beta_{zo}}\,\frac{\gamma_o^2\mu F^2}{Q} \qquad (15)$$

for a TM mode, where Q is the quality factor for the cavity (including diffractive and ohmic losses).

A contour plot showing curves of constant transverse efficiency in the F-$\mu$ plane is shown in Fig. 13 for $s=1$ and $\sigma=2$. This value for $\sigma$ was chosen as representative of actual cavities. These results were obtained by optimizing with respect to $\Delta$ subject to the constraint that the starting current be less that half the operating current, which corresponds to operation in the "soft-excitation" regime.[10] As discussed elsewhere in this paper, this constraint does not appear to apply to the present experiment: however, for the fixed Gaussian field model, it limits efficiency only at relatively large interaction lengths, in the

present case $\mu > 18$. (A larger region of hard excitation is found using the self-consistent field model, as is discussed later in this paper.) Contours of optimum $\Delta$ values corresponding to Fig. 13 are shown are shown in Fig. 14.

It is of interest to estimate the normalized parameters for the present experiment. The present experimental cavity has an effective interaction length of L=4 cm. This choice leads to good agreement between the sinusoidal field profile and the SCF theory results for threshold currents, as we discuss in Section V. Given the beam voltage, estimating the average pitch ratio $\alpha$, and correcting for space charge depression of the beam, the normalized interaction length $\mu$ can be obtained. For a typical voltage of 650 kV and for $\alpha = 1$, $\mu = 9.3$. The normalized field amplitude can be obtained by relating the peak cavity rf field amplitude to the output power. From the definition of Q, the voltage amplitude for a TE mode is given by:

$$f_o = \left[ \frac{4c^2}{\mu_o} \left(\frac{2\sigma}{\pi}\right)^{1/2} \frac{QP}{\omega L} \right]^{1/2} \qquad (16)$$

assuming a Gaussian axial rf field profile. Assuming P = 100 MW, Q = 250, L = 4 cm, and $\sigma = 2$ leads to $f_o = 1.2$ MV, corresponding to a peak field at the beam of 500 kV/cm. For a $TE_{6,2}$ mode and average beam radius of 1.2 cm, $F_o = 0.61$. These estimated parameters are denoted by the dark circle in Fig. 13 and correspond to an optimum theoretical transverse efficiency of 57%, or an electronic efficiency of 21%. The position of this point in the F-$\mu$ plane indicates that near optimum normalized field amplitude and interaction length parameters were achieved in this experiment. The principal uncertainty in determining the normalized parameters involves

the choice of $\alpha$, which is difficult to measure in the experiment. The choice of $\alpha$-1 represents an experimental estimate based on examining the change in thickness of the annular electron beam, via fluorescent screen techniques,[23] due to the effect of the "pump" magnet. It is also supported by beam trajectory calculations using the Herrmannsfeldt code,[24] and is consistent with the maximum value that may be expected, given the fairly large expected spread in electron velocity. The observation in the experiment of less than half the predicted optimum efficiency may be due in part to the lack of a method for controlling the total beam current. This is discussed further in Section V.

Substituting these values into Eq. (10), one can obtain power scaling estimates as a function of beam energy. These are shown in Fig. 15 for several TE modes.

One of the remaining theoretical issues is the influence of space charge on gyrotron operation. A preliminary discussion of the effects of space charge on the linear gyrotron interaction is given by Antonsen et al.[25] Their general conclusion is that ac space charge will tend to enhance the electron phase bunching, and therefore to increase the linear growth rate of the gyrotron instability. They also find that the general effect of dc space charge is to broaden the resonance by producing a spread in gyrofrequencies, and therefore to degrade the overall efficiency of a gyrotron oscillator. These effects have also been studied theoretically by Uhm and Davidson.[26] However, a detailed calculation of the effects of space charge on the predicted gyrotron efficiency remains to be performed. The presently available gyrotron codes[27] treat the extraction of energy from single electrons transiting the gyrotron cavity in the self-consistent rf electric and magnetic fields, and do not address

this effect.

A second issue is to understand gyrotron operation in the presence of a rapid variation of the kinetic energy of the electron beam on the time scale of the "fill time" of the gyrotron cavity. This is discussed further below.

## V. Discussion

The time-dependence of the voltage waveform is of concern both in optimizing the power and efficiency, and in making a careful comparison with the predictions of theory. Typically, the magnetic field is adjusted to produce a 35 GHz microwave peak coincident with the first diode voltage maximum, as illustrated in Fig. 2. Depending on the exact values of the magnetic field and the voltage waveform, either a single ~20 nsec wide peak at the voltage maximum, or two narrow (~10 nsec) peaks with a dip in the middle and a total width of ~20 nsec, enclosing the voltage maximum, are experimentally observed. (If the magnetic field is reduced, 35 GHz emission will begin to occur at the second voltage maximum as well.) The typical 20 nsec single microwave pulse measured at the crystal detectors would imply experimental operation through an approximate 25% variation in operating voltage. However, both the gyrotron operation and the experimental diagnostics have finite response times. In the case of the gyrotron, the effect of a voltage ramp on the nonlinear behavior of the gyrotron interaction involving a cavity that already contains strong microwave electric fields due to the start of oscillation at 35 GHz is hard to predict without a time-dependent gyrotron code. Furthermore, the response of the diagnostics is estimated to be 2-3 nsec, a time interval

over which the voltage excursion may exceed 5%.

Thus, the exact peak of the voltage waveform is not the only relevant voltage for purposes of comparing theory to experiment. In fact, the data of Fig. 5 correspond to a peak electron kinetic energy of ~735 keV. The experimentally optimum magnetic field of 23.8 kG is detuned by ~22% from exact resonance at 35 GHz, approximately 50% more than the predicted optimum detuning, and well out of the usual tuning range for the interaction. A reasonable supposition, in light of this discrepancy in the magnetic fields predicted to optimize operation as a function of beam kinetic energy, is that 35 GHz oscillation starts at some threshold current and voltage during the risetime of the first voltage maximum, persists over some portion of the remaining risetime, perhaps up to the voltage maximum, and then continues over a second interval during the decrease in voltage from the first voltage maximum.

The tuning range evident in Fig. 8 is related to the range of magnetic fields for which the 35 GHz $TE_{-62}$ mode will start oscillation, and for which oscillation will persist for long enough to reach high power levels. If the upwards voltage excursion is too great, the large microwave fields at 35 GHz will no longer extract sufficient energy from the electron beam to maintain themselves against cavity losses. Assuming no further coupling between the electron beam and the 35 GHz microwave fields, the cavity microwave fields will then decay exponentially with a characteristic time constant of $Q/\pi f$, where f is the operating frequency. This may permit a second mode at a different frequency to start oscillation. To obtain a qualitative understanding of Fig. 8, threshold current behavior as a function of beam voltage has been calculated for modes encountered during the rise of the voltage pulse.

These calculations are shown in Fig. 16 for magnetic fields of 22, 24, and 26 kG. The estimated instantaneous beam current as a function of voltage is also shown, assuming that current scales as $V^{1.33}$, which comes from calculating the space-charge-limited current as a function of voltage in the vicinity of the diode. (The effect of voltage-dependent loss of current, due to the effects of the "pump" magnet, are not included in this scaling.) In order to calculate the starting currents of the various modes, it is assumed that beam $\alpha$ scales linearly with voltage, a result that is derived from single particle simulations of the effect of the "pump" magnet. (The exact position of the beam line as well as the starting current for each mode are of course sensitive to the scaling assumptions for current and $\alpha$ as a function of voltage.) It is also assumed that the cavity Q for each mode scales as $\omega^2$, with the Q for the $TE_{\pm 62}$ modes fixed at 250. (Minimum diffraction Q for an $\ell$=1 mode near cutoff in a gyrotron cavity is given by $4\pi(L/\lambda)^2$, where $\lambda$ is the free-space wavelength associated with the operating frequency.) Start-up for a specific mode presumably begins when the beam current line intersects the threshold curve of a particular mode, and proceeds at a rate determined by the amount by which the beam current exceeds the starting current. The mode will continue to grow during the time the beam voltage waveform (see Fig. 2) sweeps the beam line through the coupling curve. The first mode to start oscillation and to reach high power should suppress other modes until coupling to this mode is lost through voltage detuning. This hypothesis remains to be verifed by time-dependent code simulations. By this argument, stable operation is expected in the $TE_{-62}$ mode at 24 kG, while 22 and 26 kG represent cases, as seen in Fig. 8, in which high power operation in this mode is not achieved. At 26 kG, the $TE_{-62}$ modes would

be suppressed by the earlier start of the $TE_{-72}$ mode, and at 22 kG, coupling to the $TE_{-62}$ mode would be lost at relatively low voltage compared to the peak voltage in the Febetron pulse.

This phenomenon of starting the $TE_{-62}$ mode at low voltage and tuning through it as the voltage rises is further examined in Fig. 17, which plots starting current and isopower curves as a function of beam voltage for the magnetic field and beam radius of Fig. 5. Assuming that no other modes interfere, the $TE_{-62}$ mode should start oscillation at 480 to 500 keV and continue oscillation as the energy tunes upward with time to at least 700 keV. The solid lines in Fig. 17 are calculated assuming a sinusoidal rf field profile in the cavity, with length 4 cm. The dashed line and the two marked points are calculated using a self-consistent rf-field profile in the cavity. The dashed line gives the threshold while the dots indicate optimum efficiency operating points. These self-consistent calculations generally validate the simpler sinusoidal calculations, particularly in the area of start-oscillation current thresholds. A natural feature of a high voltage gyrotron experiment with a finite risetime is that the voltage tuning illustrated in Fig. 17 occurs naturally, and in fact the interaction tunes itself naturally into the hard excitation regime, i.e. the regime of operation in which the starting current exceeds the operating current, and the highest efficiences are typically observed. This effect also enhances stability by allowing the mode to start oscillation under conditions of high growth rate (low threshold current). When the resonance enters the highly detuned maximum efficiency regime, the interaction has already become strongly nonlinear, and the start-up of competing modes with higher linear growth rates is suppressed. The two points plotted, at 650 and 700 keV, correspond to

optimum efficiency points with output powers of 137 MW and 275 MW, respectively, calculated from the self-consistent model. Figure 17 suggests that coupling may not persists to the exact peak of the voltage waveform (~735 keV, after correcting for space charge depression), but the short duration of the voltage excursion beyond 700 kV (see Fig. 2) might mask this effect experimentally.

Fig. 18 presents two plots of efficiency versus electron beam current, assuming $B_o$=24 kG, V=650 keV, and beam $\alpha$=1. These curves are calculated assuming a self-consistent rf field profile in the experimental gyrotron cavity. Curves are calculated assuming either a cold beam ($\Delta v_z$=0), or a large velocity spread ($\Delta v_z/v_z$=20%). In each case, the start oscillation threshold is illustrated: operation to the left of the start oscillation threshold corresponds to a region of hard excitation, in which oscillation would not start, but which could be reached either by lowering the gyrotron current once oscillation had begun, or in the case of this experiment, by starting oscillation at lower voltages. Generally, when the curve is double-valued, the higher value corresponds to stable oscillation. The choice of 650 keV for these calculations corresponds to somewhat less than the highest beam kinetic energy of ~735 keV for a normalized beam radius of 0.75, but was chosen in light of the data of Fig. 17, and the general consideration that the exact peak of the voltage waveform occurs for a very short time (see Fig. 2). As expected in a gyrotron oscillator, these calculations are not highly sensitive to velocity spread. The maximum theoretical warm beam efficiency is about 25% more than twice the observed efficiency. However, the highest efficiencies were obtained at lower beam currents than those used in the experiment, suggesting that the cavity was somewhat overdriven. The

predicted efficiency at the experimental current of 1600 A, which corresponds to the data of Fig. 5, is in reasonable agreement with the observed power levels. Figure 18 suggests that comparable powers at higher efficiences could be achieved at lower beam currents. However, the principal experimental goal was to maximize peak power rather than to optimize efficiency. Since the basic diode geometry controlled the total emitted current of ~3.5 kA, operation at lesser values of the beam current (e.g., the ~1.6 kA that was employed to produce the optimum power) was achieved as a side effect of the "pump" magnet that was used to provide a high beam transverse momentum. Furthermore, in order to perform an experimental scan of the emission corresponding to a particular set of operational parameters, it was necessary to operate with parameters for which the operation of the gyrotron was most stable to small variations, due to the problem of shot-to-shot reproducibility of the experimental discharges. Operation of the gyrotron at the substantially lower current (~600 A) that is predicted to optimize the efficiency of the interaction could only be achieved by increasing the magnitude of the nonadiabatic change in axial magnetic field induced by the "pump" magnet, resulting in the loss of additional beam current between the diode and the gyrotron cavity--at some point, this process is expected to be highly deleterious of electron beam quality, and in addition, the problem of reproducibility was significantly increased. Nevertheless, there was some limited evidence that comparable peak powers might be achieved at somewhat (30-50%) lower operating currents. (An attempt to use a beam mask in the vicinity of the diode to lower the beam current by scraping the edge of the beam was unsuccessful, since it was very difficult to successfully scrape an azimuthally symmetric fraction of a thin annular beam. The

presence of a beam scraper also tended to lower the diode impedance and therefore to decrease the operating voltage of the experiment.)

Voltage-dependent start-up effects may explain the large detuning illustrated by the best fit line to the data points of Fig. 12. Figure 19 shows the calculated starting currents versus magnetic field for first harmonic $TE_{mn1}$ modes occurring between 15 and 35 kG. These starting currents are obtained using a small signal theory and computer code for the gyrotron oscillator based on linearized Vlasov theory,[28] and assuming a sinusoidal cavity rf electric field profile with a length of 4 cm, a cavity Q of 250, a beam voltage of 450 keV, an $\alpha$ of 1, and a normalized beam radius of 0.67. These calculations are considered to be essentially equivalent to a small signal analysis based on Eqs. (1a) and (1b). This has been verified numerically. The beam voltage of 450 keV assumed for these calculations was selected to place the minima as a function of magnetic field for the various $TE_{\pm m2}$ mode starting current curves along the experimental "best fit" line of Fig. 12. This figure illustrates why it is possible, for this normalized beam radius, to tune the gyrotron between the various $TE_{m2}$ modes by varying the cavity magnetic field, since they are generally the lowest starting current modes. (Similar tuning of a gyrotron in a $TE_{m2}$ family of modes has recently been reported elsewhere in a long pulse gyrotron employing thermionic cathode technology.[8]) It also illustrates why it is increasingly difficult to observe standing modes below m=6, since the starting current for the $TE_{+m2}$ mode begins to greatly exceed that for the $TE_{-m2}$ mode, while for larger m values, they are approximately equal. However, it is important to note that while the exact starting voltage for a mode as a function of axial magnetic field is known approximately for the time-resolved 35 GHz data of Fig. 8, it is

unknown experimentally for the time-integrated breakdown data of Fig. 12. A higher or lower voltage will have the general effect of translating the starting current curves for the various modes to higher or lower magnetic fields, without strongly affecting the relationships between the various curves. These calculations therefore suggest that as the beam current, voltage, and $\alpha$ increase with time during the voltage waveform, up to the final beam kinetic energy of ~725 keV, the first mode to reach high power will typically start at about 450±50 keV. (If a higher frequency mode begins to be excited at lower beam $\gamma$, the beam presumabably detunes from the mode before high levels of rf electric field are reached in the gyrotron cavity, as suggested in the discussion of Fig. 16.)

In summary, a 35 GHz gyrotron oscillator has successfully operated in a $TE_{62}$ "whispering-gallery" mode at a power level of approximately 100 MW and an efficiency of approximately 8%. Its frequency has been tuned over almost a factor of two at high power through variation of the resonant magnetic field in the region of the microwave cavity. This tuning has been accomplished through operation of the gyrotron in a family of $TE_{m2}$ modes ranging from m=4 to m=10 by varying the cavity magnetic field while maintaining approximately constant beam parameters. Operation has generally agreed with the predictions of conventional gyrotron theory, with special effects due to high beam $\gamma$ being observed.

The principal discrepancy between theory and experiment is in the area of maximum efficiency, with the predicted maximum efficiencies typically exceeding the experimental values by a factor of ~2. This disagreement is attributed principally to two factors. On the theoretical side, the effects of space charge would be expected to degrade the overall efficiency, but theoretical models including these effects are not yet

available. A second concern is the rapid time-variation of the voltage pulse, since we have been limited to the use of steady-state gyrotron models to analyze an experiment in which the time-variation of the voltage waveform would appear to have significant experimental consequences. On the experimental side, it has proved difficult to operate the experiment at the levels of current that are predicted to optimized the efficiency in the present experimental cavity. Also, there is a continuing concern with the velocity spread of the electron beam, since there are indications that the present electron beam is given high transverse momentum at the expense of beam quality. Studies are continuing on the formation of higher quality electron beams to drive more efficient gyrotron interactions.

An important constraint on the experiment is its present operation at the maximum charge voltage of the Febetron pulser, which implies that any lowering of the diode impedance will occur at the expense of operating voltage. This places significant constraints on the diode design, and requires operation in an essentially "foilless" configuration, i.e. with the cylindrical drift tube serving as the anode. To relax this constraint in order to have better control of the beam formation process, plans are proceeding to continue the experiment on a higher voltage, lower impedance pulseline accelerator, which will substantially increase the experimental flexibility in the area of beam formation as well as making possible operation at still higher beam energies and with a substantially improved voltage waveform. This is expected to permit future gyrotron operation at significantly higher power levels than are reported in this paper.

## Acknowledgments

We gratefully acknowledge helpful discussions with Dr. Kwo Ray Chu and Dr. A.T. Lin. In addition, we are grateful to Dr. Chu for providing an early version of the computer code used to perform the mode startup calculations shown in Fig. 16. We are also grateful for the computational assistance provided by Lisa Lagrand. This work was supported by the Office of Naval Research and by the Office of Innovative Science and Technology of the Strategic Defense Initiative Organization.

## References


1. V.L. Granatstein, Int. J. Electron. 57, 787 (1984).
2. K. Felch, R. Bier, L. Fox, H. Huey, L. Ives, H. Jory, N. Lopez, J. Manca, J. Shively, and S. Spang, Int. J. Electron. 57, 815 (1984).
3. V.L. Granatstein, P. Vitello, K.R. Chu, K. Ko, P.E. Latham, W. Lawson, C.D. Striffler, and A. Drobot, IEEE Trans. Nucl. Sci. NS-32, 2957 (1985).
4. V.L. Granatstein, M. Herndon, P. Sprangle, Y. Carmel, and J.A. Nation, Plasma Phys. 17, 23 (1975).
5. S.N. Voronkov, V.I. Krementsov, P.S. Strelkov, and A.G. Shkvarunets, Zh. Tech. Fiz. 52, 106 (1982) [Sov. Phys. Tech. Phys. 27, 68 (1982)]. Also, V.V. Bogdanov, S.N. Voronkov, V.I. Krementsov, P.S. Strelkov, V.Yu. Shafer, and A.G. Shkvarunets, Zh. Tekh. Fiz. 53, 106 (1983) [Sov. Phys. Tech. Phys. 28, 61 (1983)].
6. A.D.R. Phelps, T. Garvey, and A.S. Hasaani, Int. J. Electron. 57, 1141 (1984).
7. V.A. Flyagin, A.G. Luchinin, and G.S. Nusinovich, Int. J. Infrared Millimeter Waves 4, 629 (1983).
8. K.E. Kreischer, S. Spira, and R.J. Tempkin, in the Conference Digest of the Eleventh International Conference on Infrared and Millimeter Waves, Tirrenia, Pisa, Italy, October 20-24, 1986, pp. 229-231.
9. S.H. Gold, A.W. Fliflet, W.M. Manheimer, W.M. Black, V.L. Granatstein, A.K. Kinkead, D.L. Hardesty, and M. Sucy, IEEE Trans. Plasma Sci. PS-13, 374 (1985).
10. M.A. Moiseev and G.S. Nusinovich, Izv. Vyssh. Uchebn. Zaved., Radiofiz. 17, 1709 (1974) [Radiophys. Quantum Electron. 17, 1305 (1974)].

11. B.C. DeLoach, Jr., IRE Trans. Microwave Theory Tech. 9, 130 (1961).

12. See L.J. Chu, J. Appl. Phys. 11, 603 (1940) for a calculation of the gain of a rectangular hollow pipe, and Reference Data for Radio Engineers, 6th ed. (Howard W. Sams & Co., Indianapolis, 1981) for the relationship between gain and effective aperture.

13. A.W. Fliflet, NRL Memorandum Report 5598 (1985).

14. P. Sprangle and W.M. Manheimer, Phys. Fluids 18, 224 (1975).

15. E. Ott and W.M. Manheimer, IEEE Trans. Plasma Sci. PS-3, 1 (1975).

16. V.A. Flyagin, A.V. Gaponov, A.V. Petelin, and V.K. Yulpatov, IEEE Trans. Microwave Theory Tech. MTT-25, 514 (1977).

17. P. Sprangle and A.T. Drobot, IEEE Trans. Microwave Theory Tech. MTT-25, 528 (1977).

18. K.R. Chu, Phys. Fluids 21, 2354 (1978).

19. K.R. Chu, A.T. Drobot, H.H. Szu, and P. Sprangle, IEEE Trans. Microwave Theory Tech. MTT-28, 313 (1980).

20. V.L. Bratman, N.S. Ginzburg, G.S. Nusinovich, M.I. Petelin, and P.S. Strelkov, Int. J. Electron. 51, 541 (1981).

21. A.W. Fliflet, M.E. Read, K.R. Chu, and R. Seeley, Int. J. Electron. 53, 505 (1982).

22. A.W. Fliflet, NRL Memorandum Report 5812 (1986).

23. V.I. Krementsov, P.S. Strelkov, and A.G. Shkvarunets, Zh. Tekh. Fiz. 50, 2469 (1980) [Sov. Phys. Tech. Phys. 25, 1447 (1981)].

24. W.B. Herrmannsfeldt, Stanford Linear Accelerator Report No. 226, 1979.

25. T.M. Antonsen, W.M. Manheimer, and B. Levush, Int. J. Electron., to be published.

26. H.S. Uhm and R.C. Davidson, Phys. Fluids 29, 2713 (1986).

27. A.W. Fliflet, M.E. Read, K.R. Chu, and R. Seeley, Int. J. Electron. 53, 505 (1982).

28. K.R. Chu, Phys. Fluids 21, 2354 (1978).

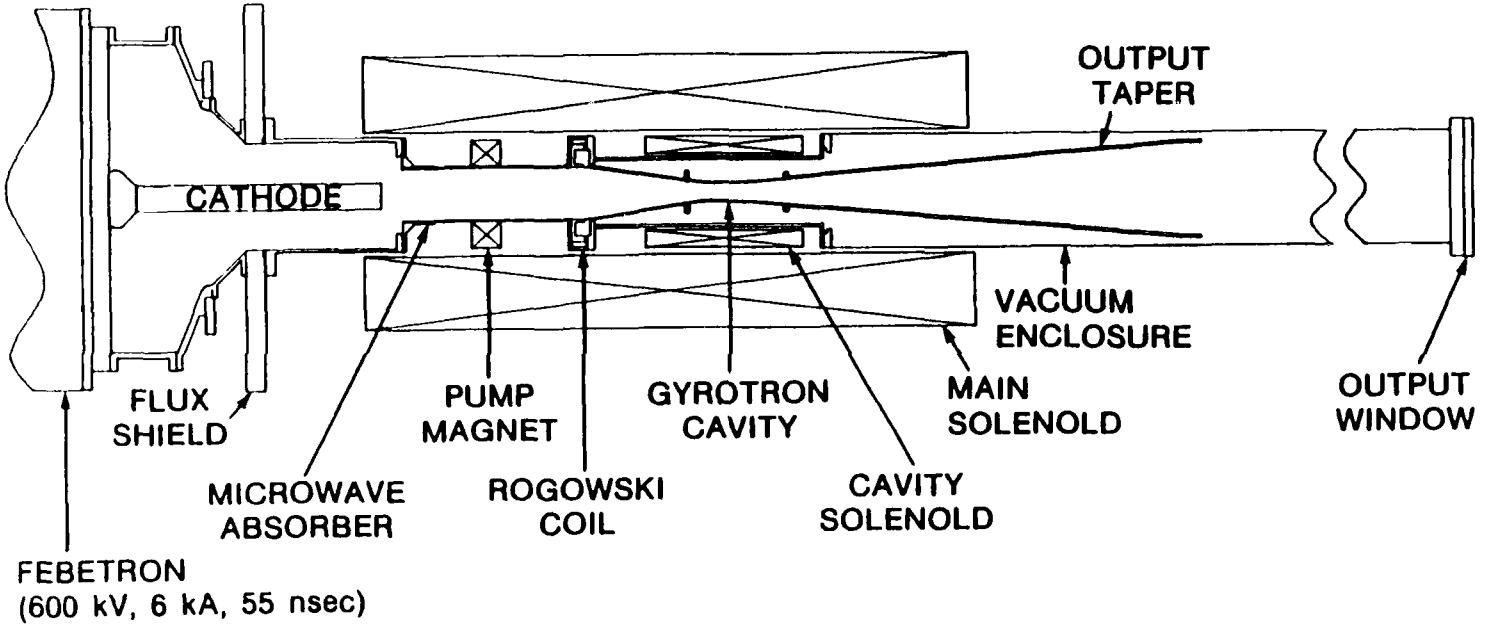


Fig. 1. Schematic diagram of the high voltage gyrotron experimental setup.

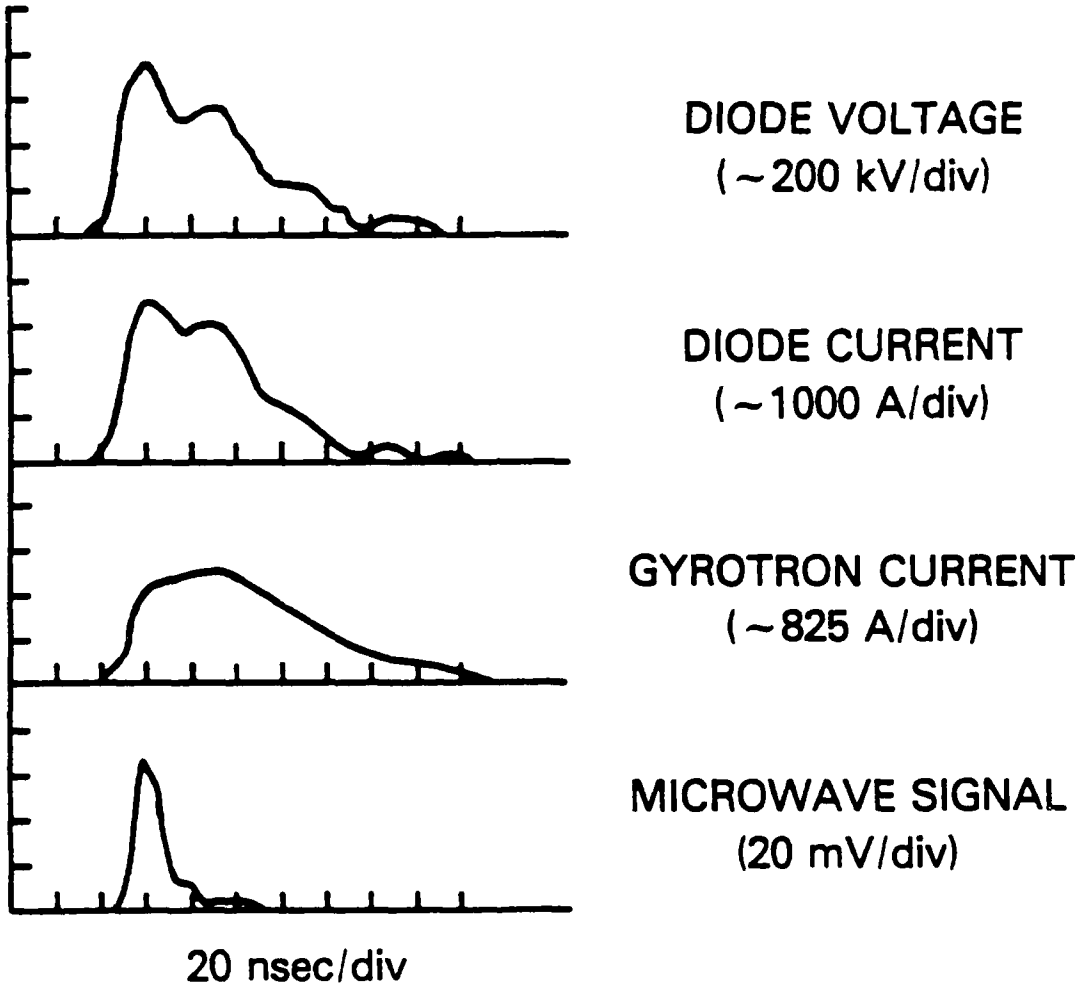


Fig. 2. Typical experimental waveforms as a function of time. (Note that the signs of the voltage and current waveforms are inverted.)

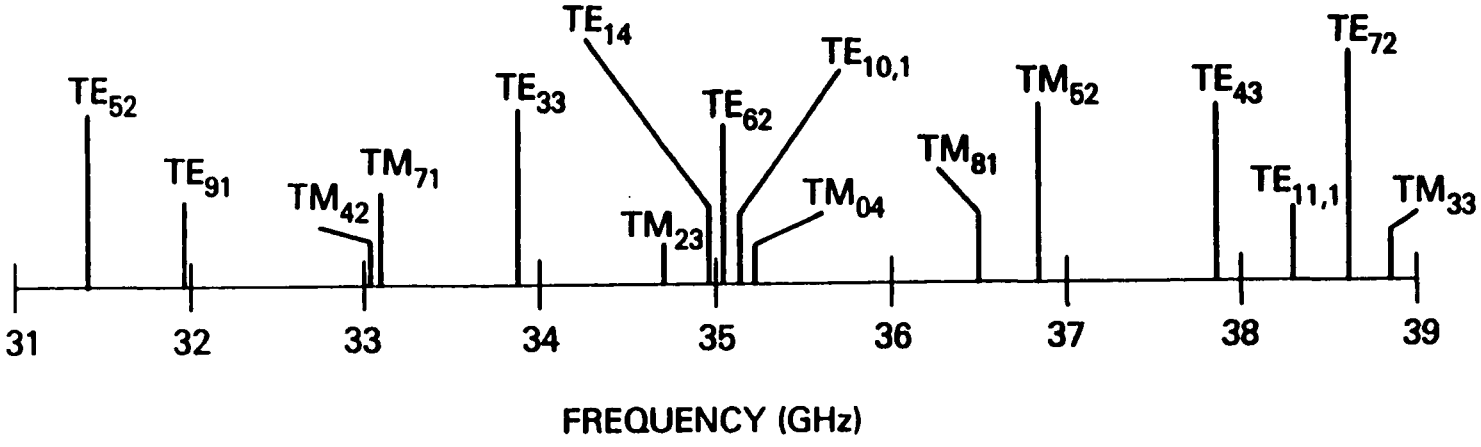


Fig. 3. Map of the $TE_{mn1}$ and $TM_{mn1}$ cavity modes in the vicinity of 35 GHz.

Fig. 4. Open shutter photograph of microwave-produced breakdown on the open end of the microwave aperture antenna in the vicinity of the output window. Gas breakdown streamers are shown extending from the edge of the waveguide aperture (right) to the output window (left).

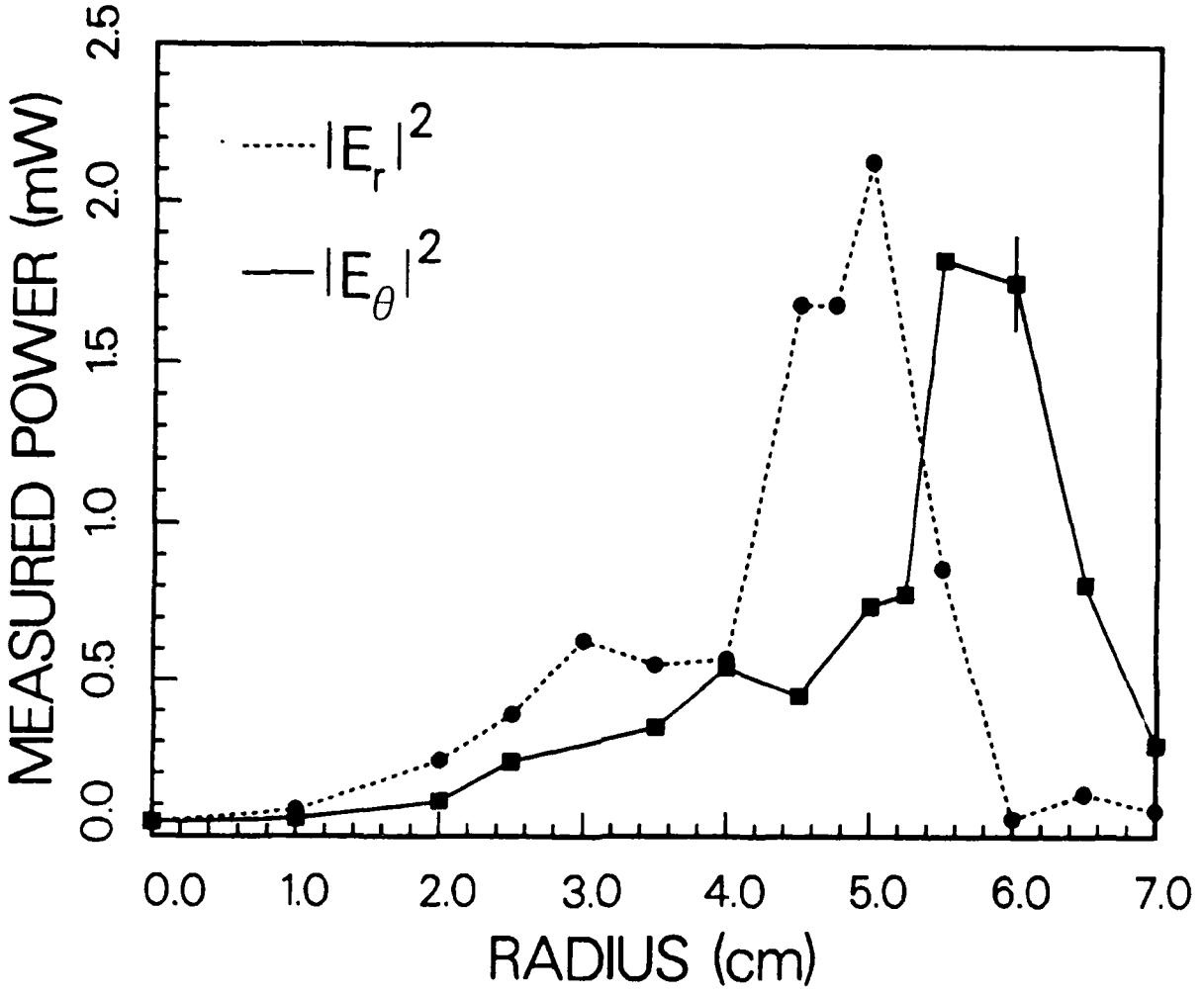


Fig. 5. Measured microwave power in radial and azimuthal polarizations vs radius across the experimental output window. A typical statistical error bar is shown.

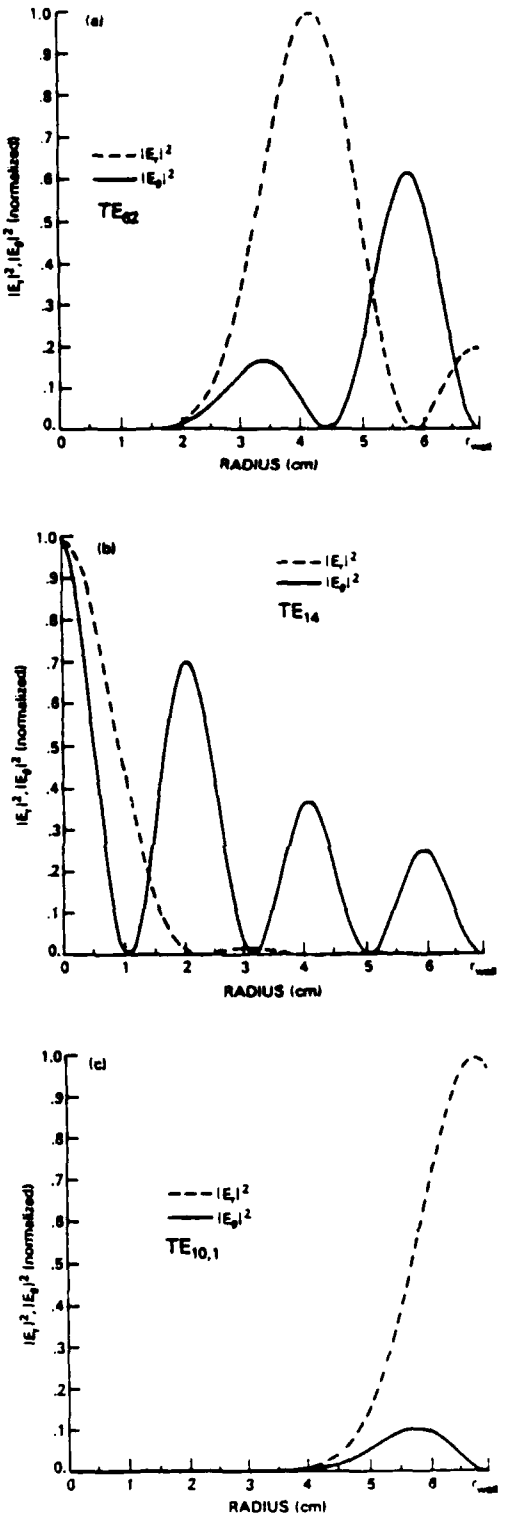


Fig. 6. Predicted mode pattern for the $TE_{62}$, $TE_{14}$, and $TE_{10,1}$ modes.

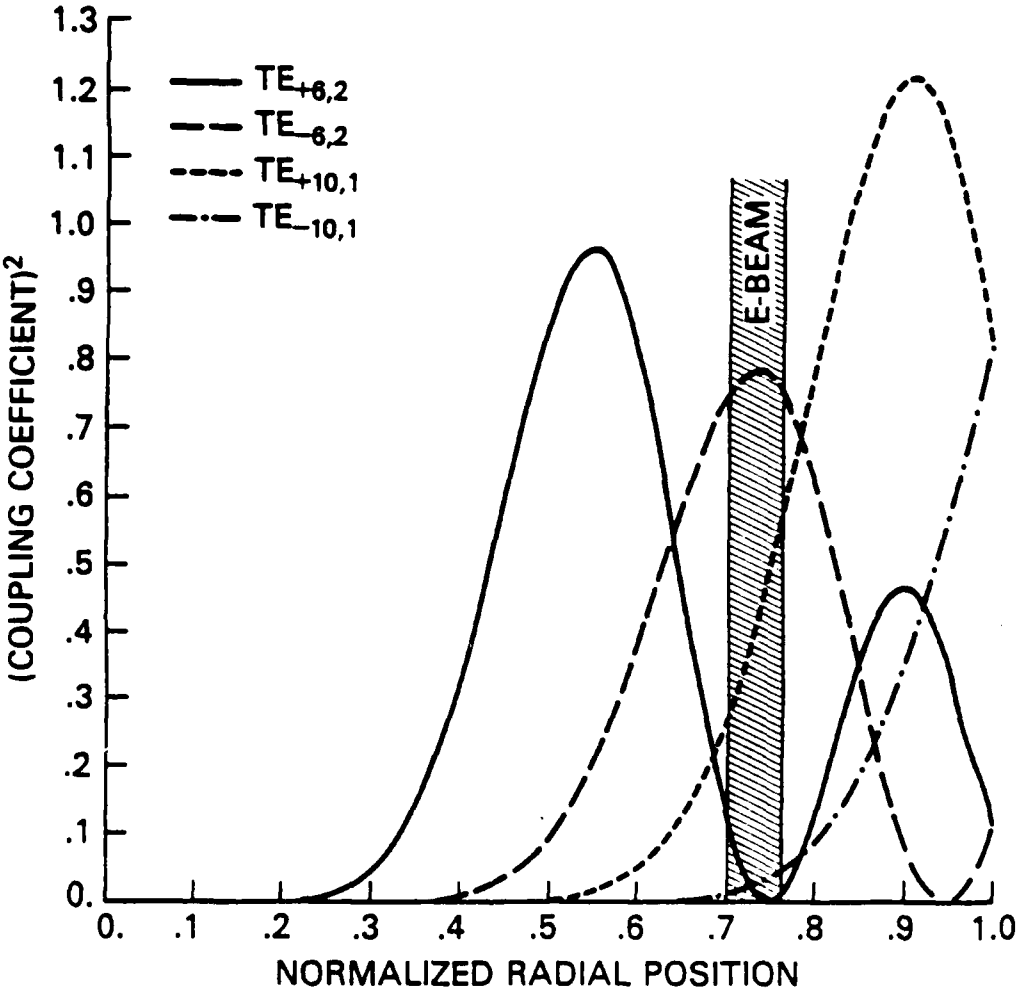


Fig. 7. Gyrotron coupling coefficients versus radius for the $TE_{\pm 62}$ and $TE_{\pm 10,1}$ modes.

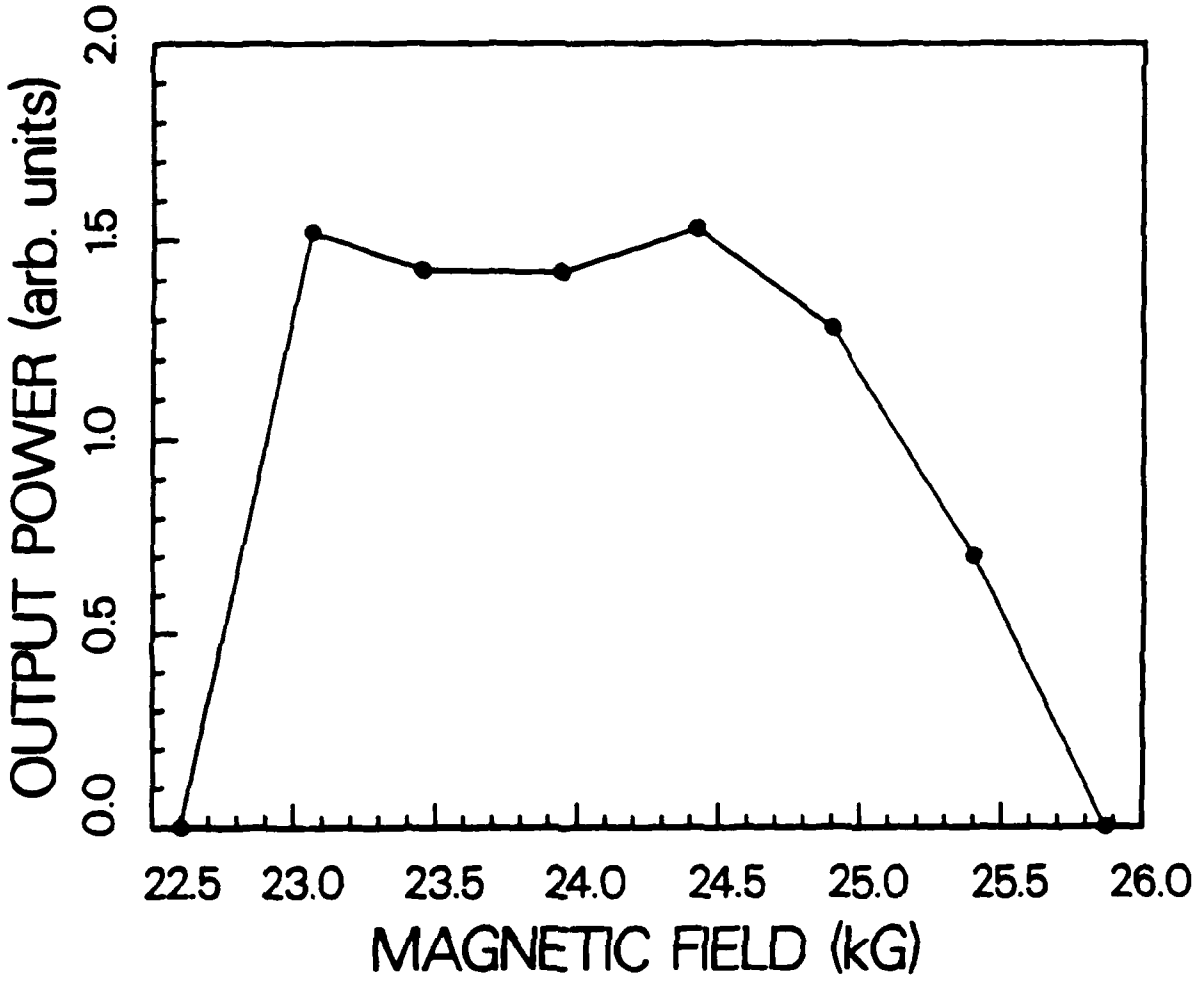


Fig. 8. Measured output power at 35.0±0.2 GHz at the radial maximum of $|E_r|^2$ for the $TE_{62}$ mode as a function of magnetic field.

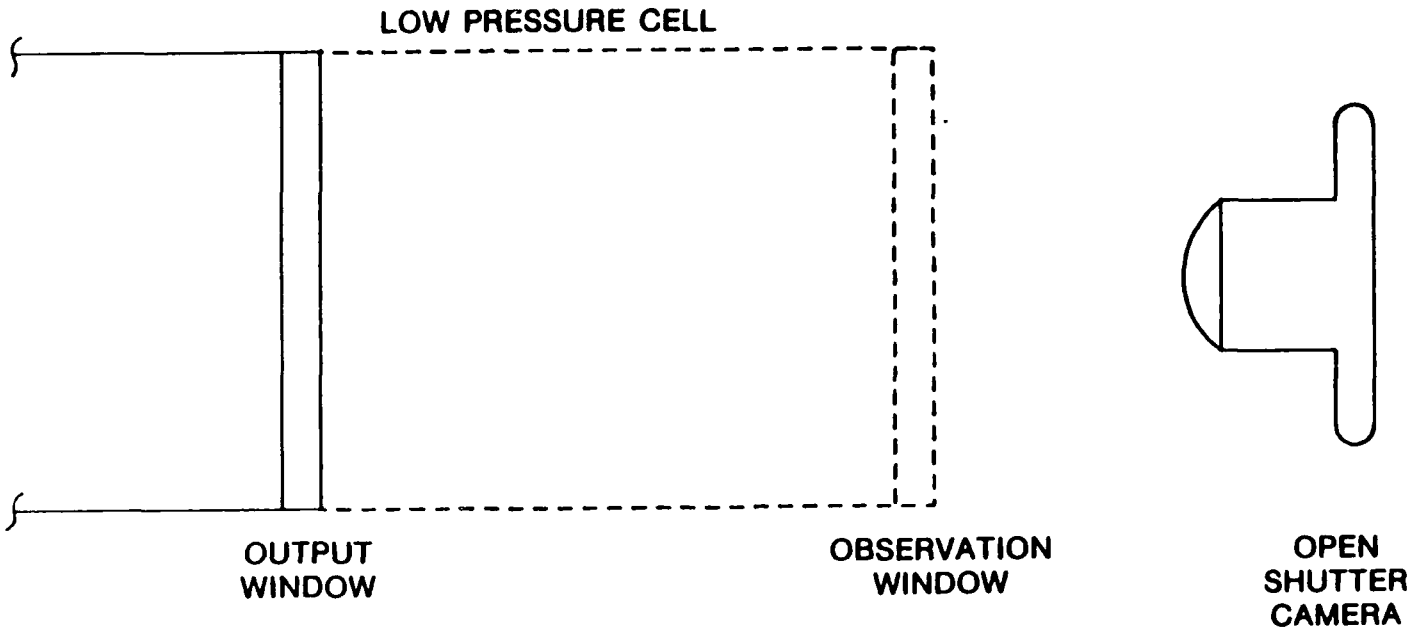


Fig. 9. Experimental setup for observation of microwave-produced gas breakdown.

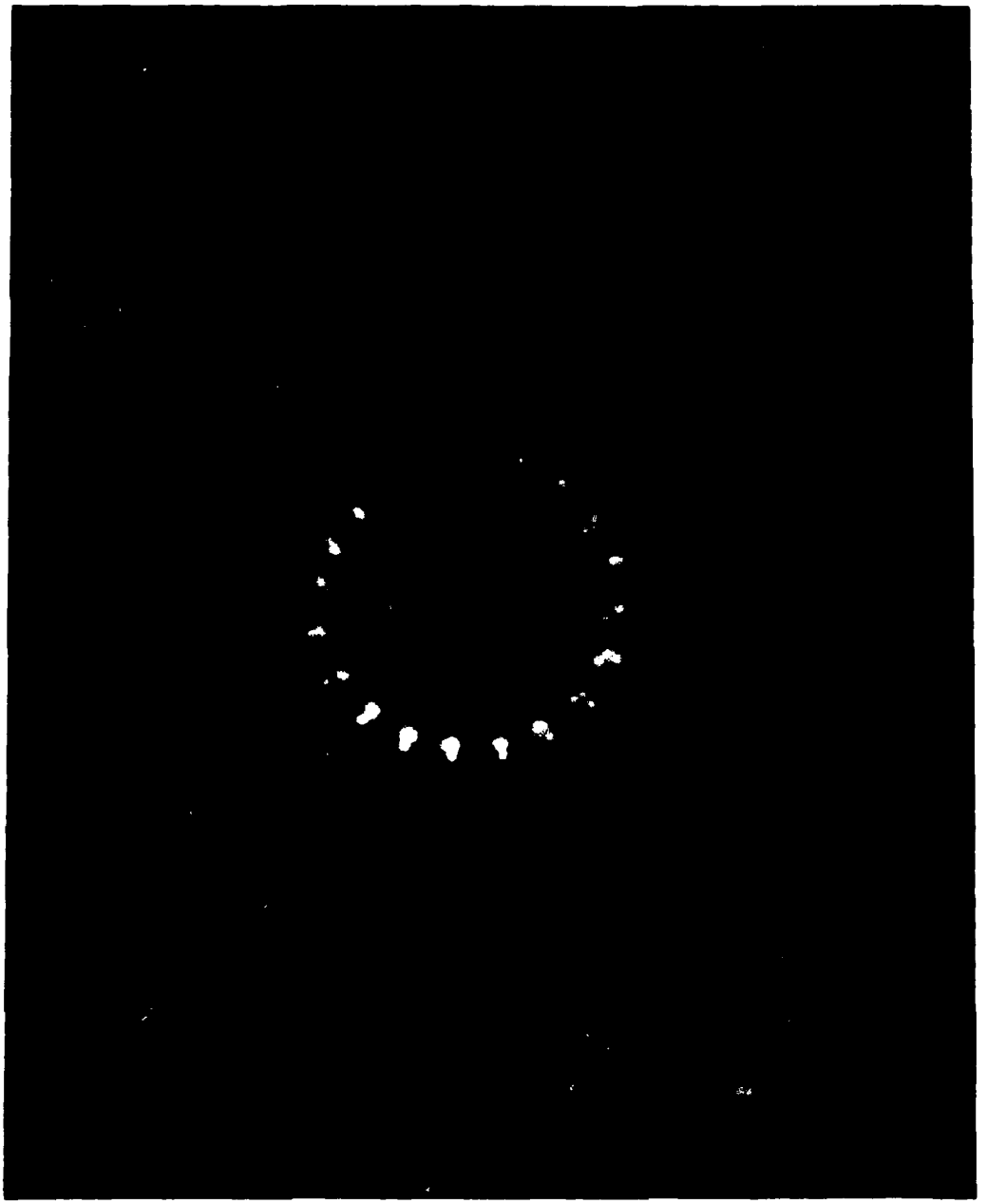

Fig. 10. End-on open shutter photograph of microwave-induced gas breakdown for $B_o$=30.3 kG, illustrating the observation of the $TE_{10,2}$ mode. (The outer halo is a reflection in the walls of the breakdown cell. Vertical and horizontal lines are cm rulings on the window face.)

Fig. 11. End-on open shutter photograph of microwave-induced gas breakdown for $B_o$=28.7 kG, illustrating the observation of the $TE_{92}$ mode.

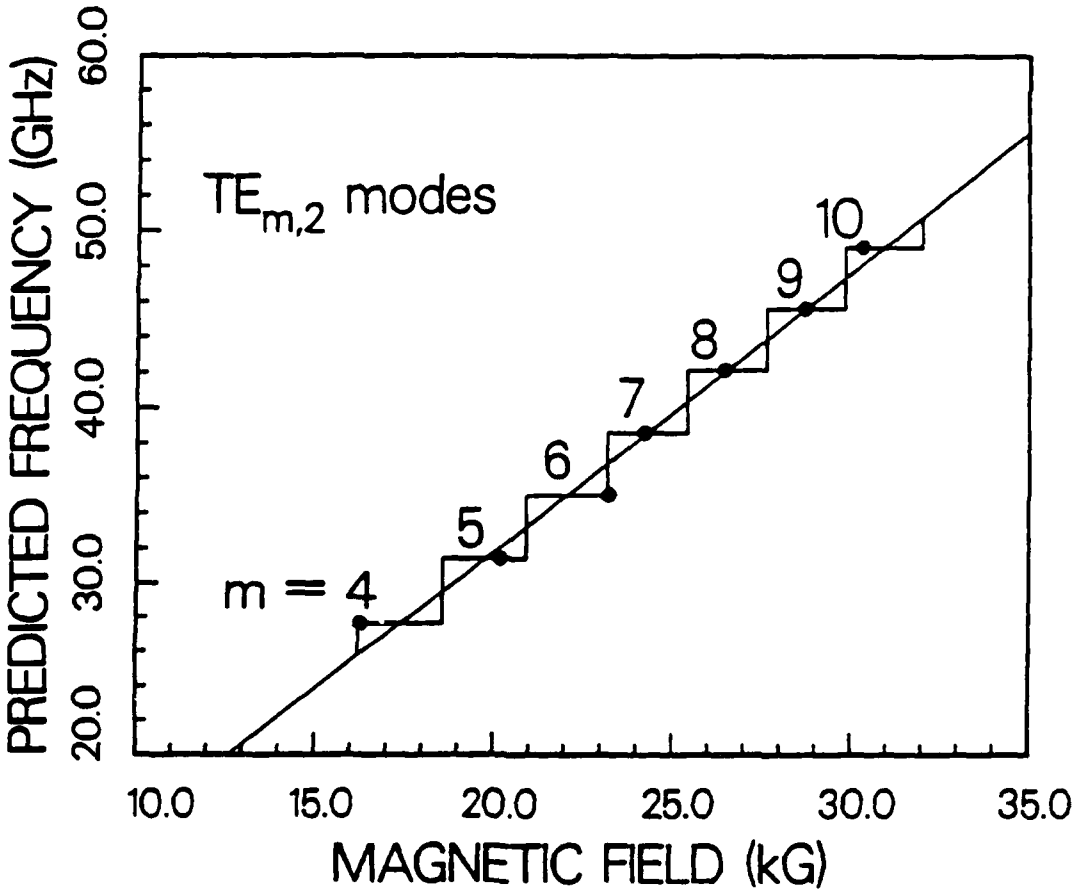


Fig. 12. Predicted frequency versus applied magnetic field for observed $TE_{m2}$ modes. The "best fit" straight line to the data points is included, as well as a "stair-step" line the corresponds to the range over which each mode should be expected to start oscillation.

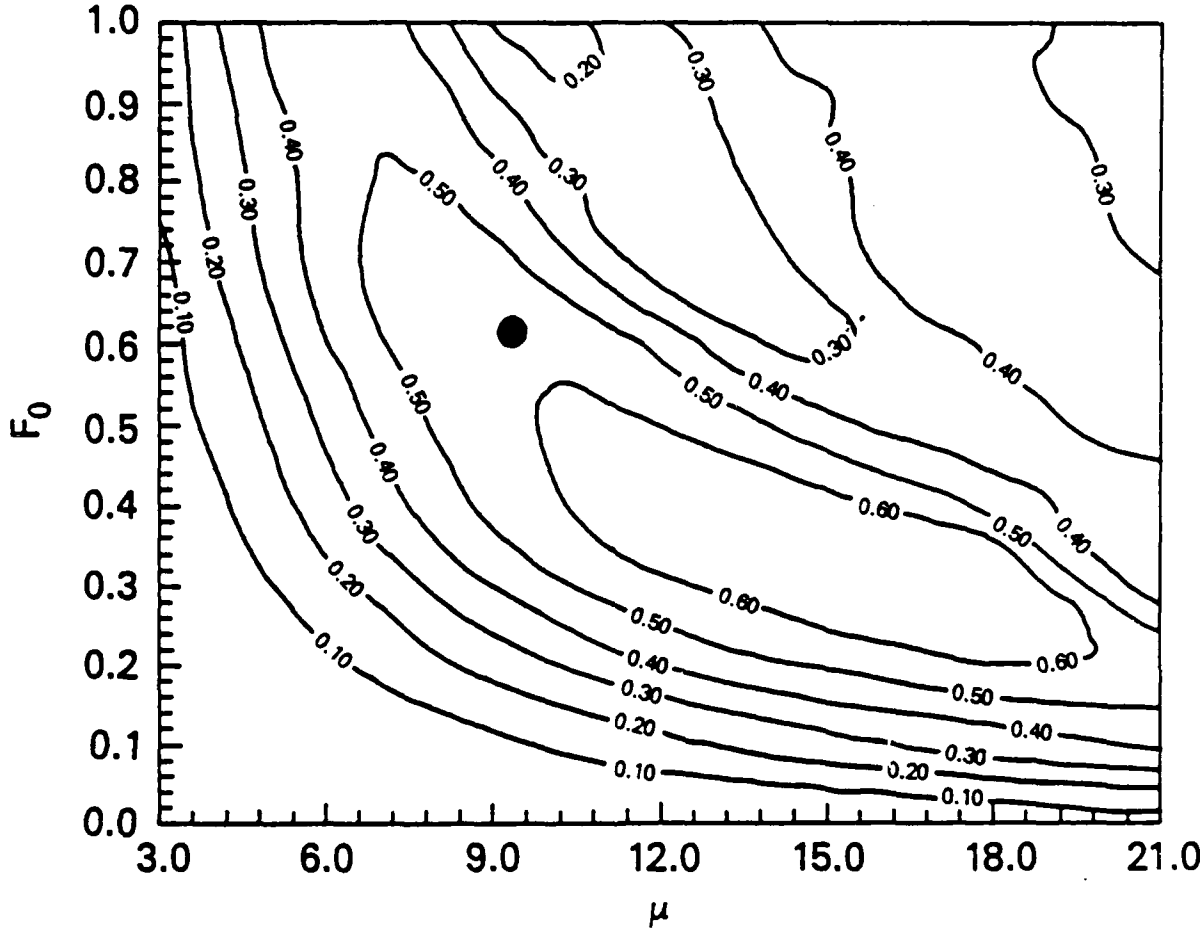


Fig. 13. Curves of constant transverse efficiency for a Gaussian axial rf-field profile and optimized $\Delta$ for $s=1$, $\sigma=2$, $I_{thr} \leq 0.5\ I_o$. The solid dot indicates the estimated experimental parameters.

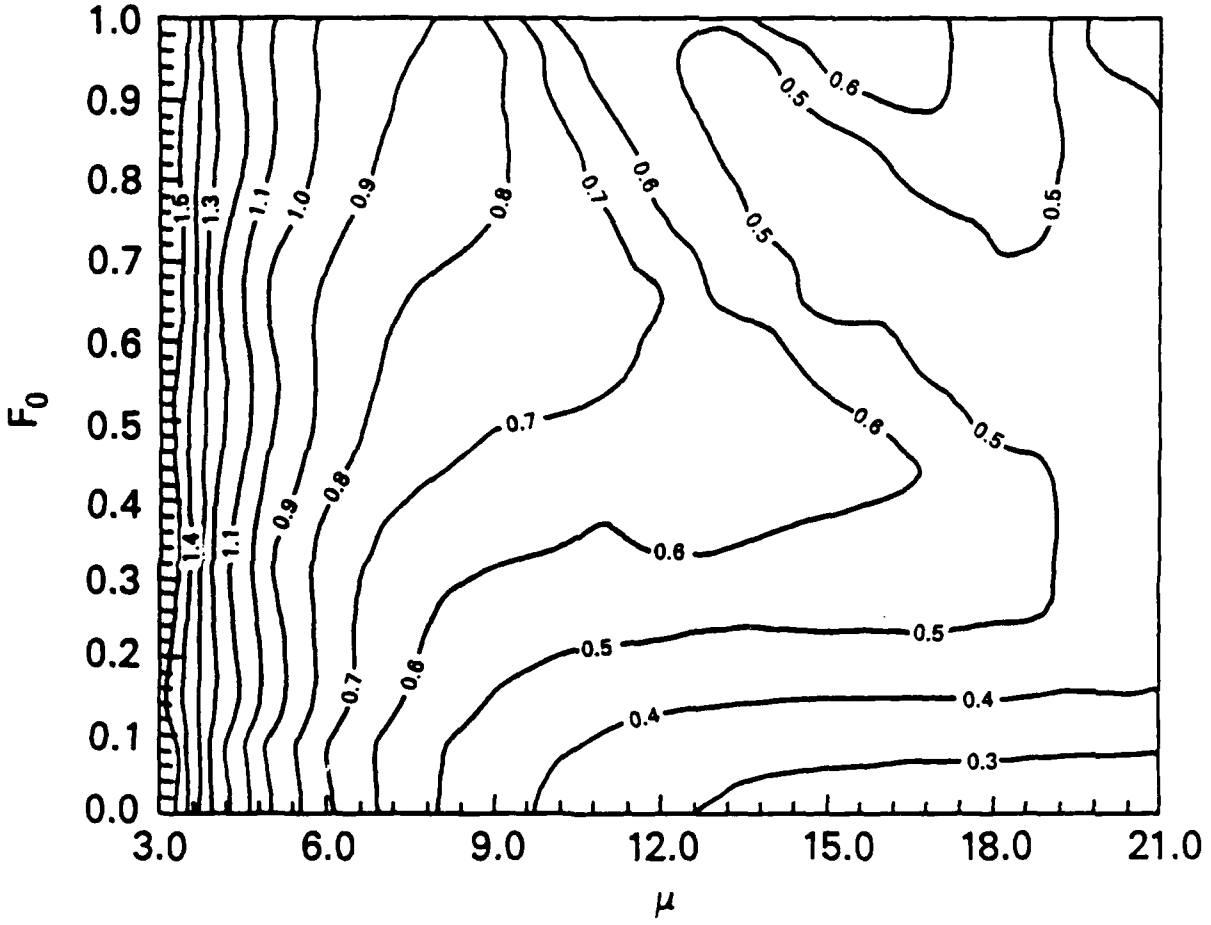


Fig. 14. Curves of optimum Δ corresponding to Fig. 12.

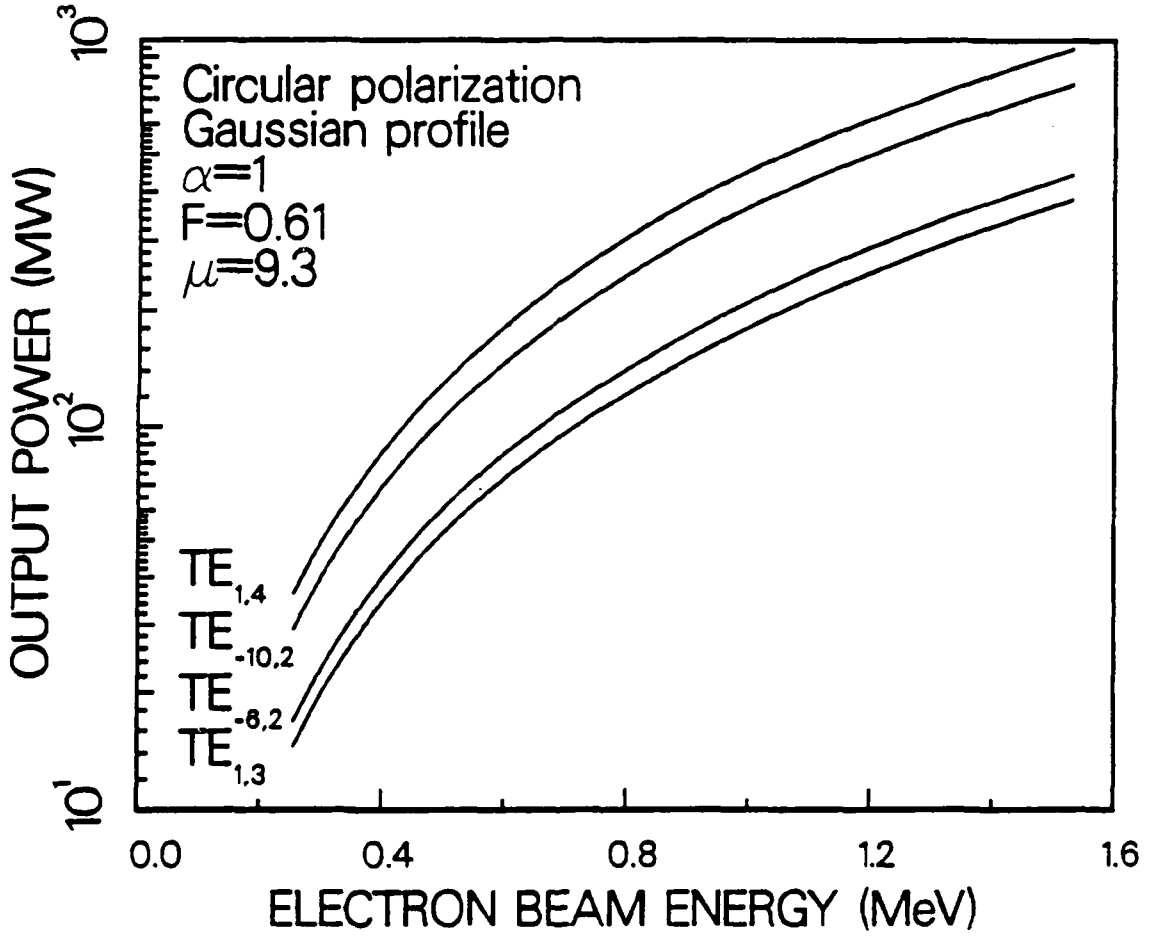


Fig. 15. Gyrotron power scaling as a function of beam energy.

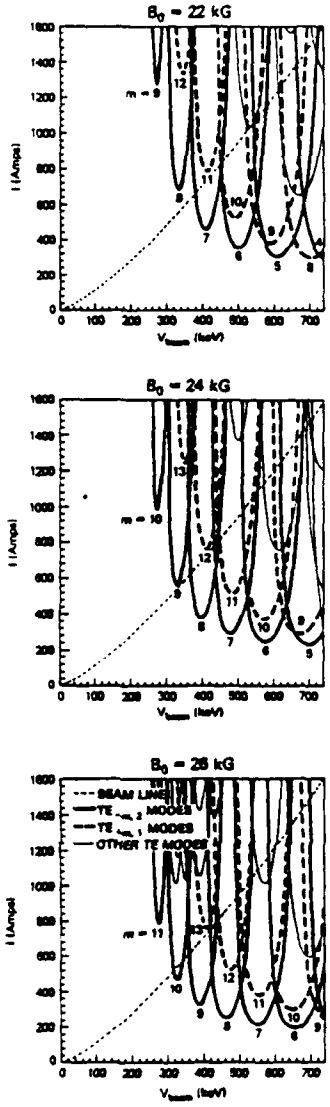


Fig. 16. Mode startup versus voltage, for $B_0$=22 kG (top), 24 kG (center), and 26 kG (bottom). The beam current is assumed to scale as $V^{1.33}$, with a maximum value of 1.6 kA at 740 keV, and the beam $\alpha$ is assumed to scale as V, with a maximum $\alpha$ of 1 at 740 keV. The Q of the $TE_{-62}$ mode is assumed to be 250, with the Q values for other modes assumed to scale as the square of the mode frequency. A normalized beam radius of 0.75 is assumed in the gyrotron cavity.

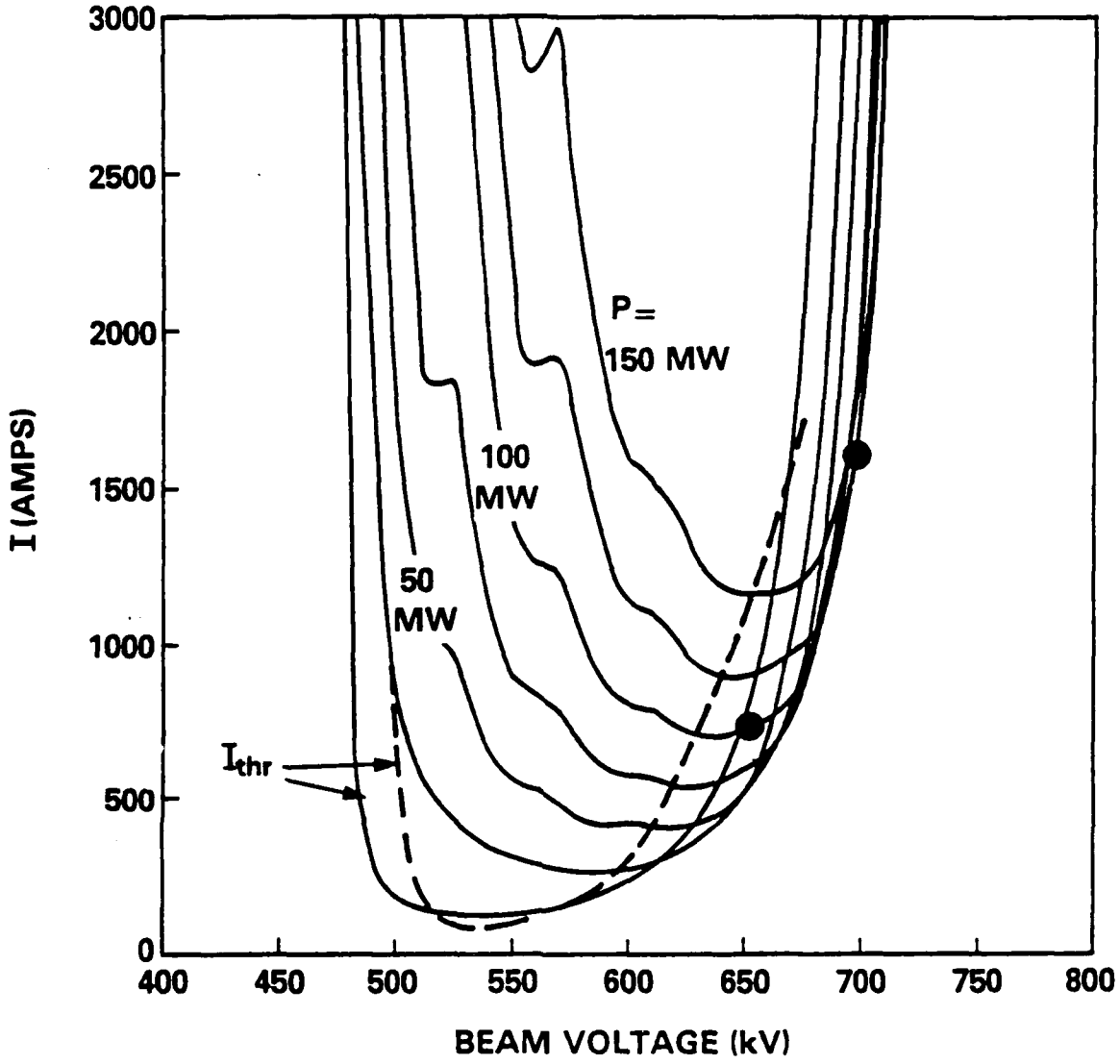


Fig. 17. Gyrotron starting current and isopower curves as a function of beam voltage for $B_o$=23.8 kG and $r_b/r_w$=0.75. The dashed line illustrates the starting current calculated by a self-consistent model of the cavity rf-fields, while the solid lines are calculated assuming a sinusoidal rf field profile with L=4 cm. The two dots indicate the predicted optimum efficiency points from the self-consist model at 650 keV and 700 keV, and correspond to 137 and 275 MW.

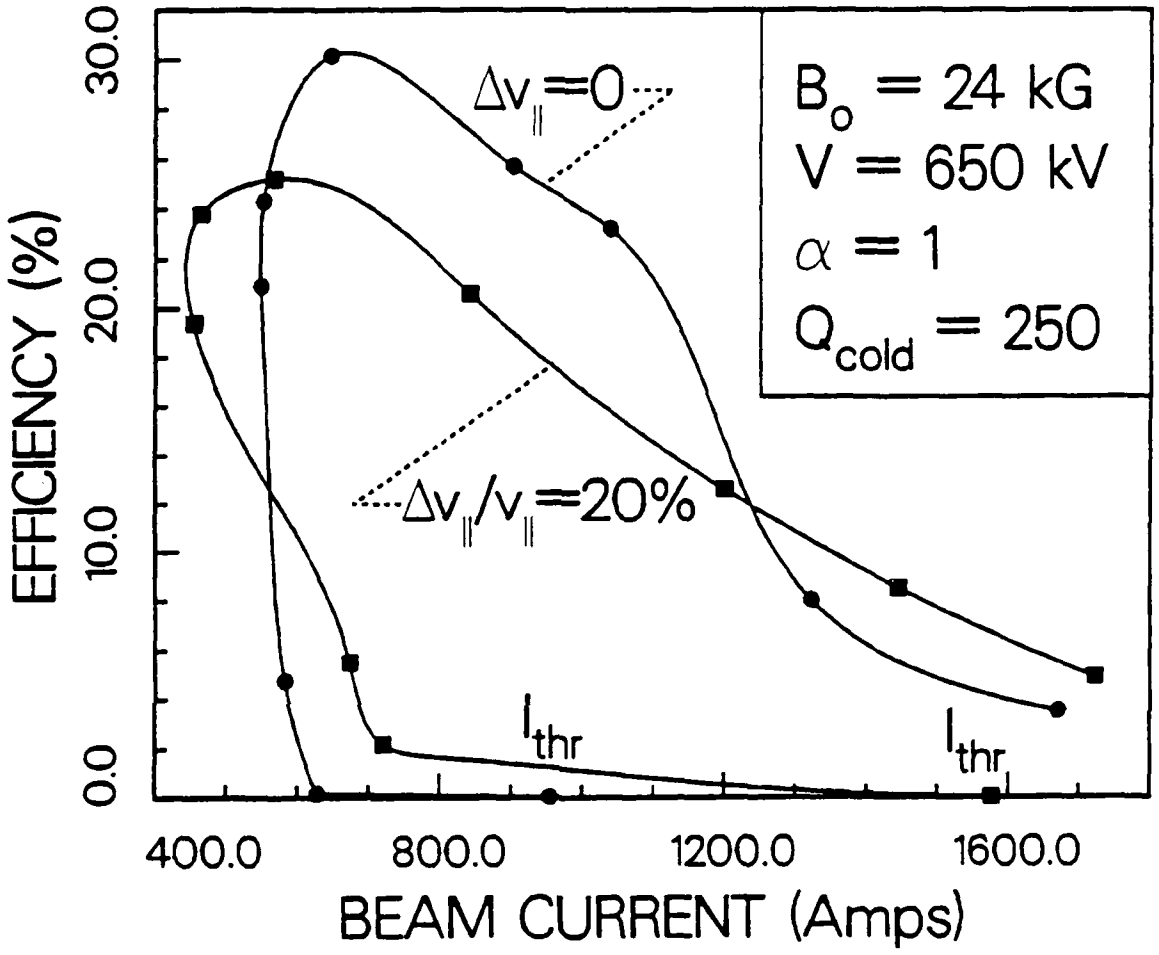


Fig. 18. Efficiency versus beam current for a $TE_{62}$ mode, calculated from a self-consistent model of the rf-field profile in the experimental cavity, and assuming $B_o$=24 kG, V=650 keV, and $\alpha$=1. Calculations are performed for the case of a cold beam (no axial velocity spread) and for a 20% spread.

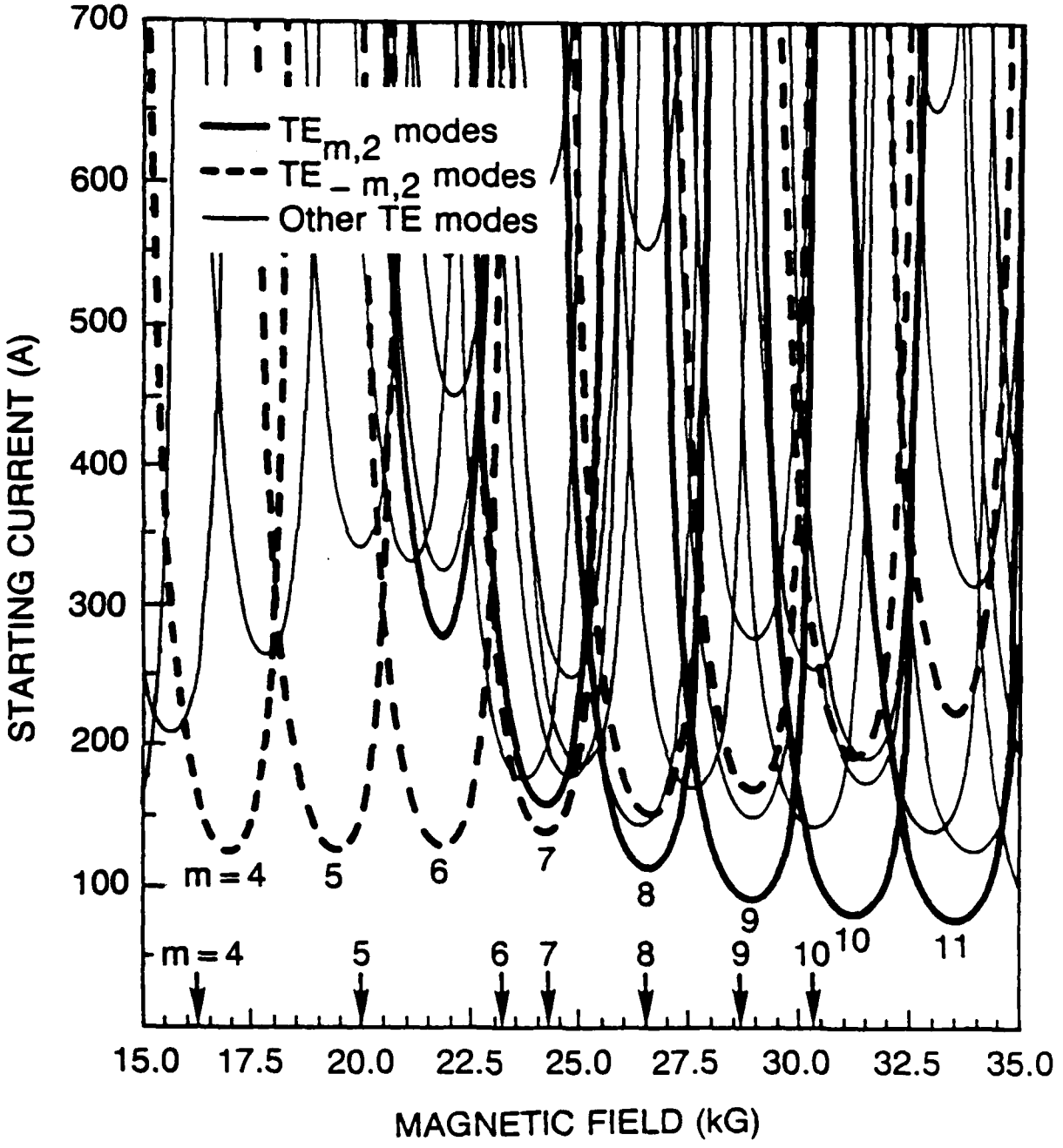


Fig. 19. Predicted gyrotron starting current versus magnetic field for the $TE_{\pm m21}$ modes for V=450 keV, $\alpha$=1, Q=250, and normalized beam radius of 0.67. Other $TE_{mn1}$ modes are also shown. The magnetic field at which the various $TE_{m2}$ modes were observed experimentally via breakdown diagnostics are indicated by arrows.

## 4740 DISTRIBUTION LIST

Air Force Avionics Laboratory
AFWAL/AADM-1
Wright/Patterson AFB, Ohio 45433
Attn: Walter Friez — 1 copy

Air Force Office of
Scientific Research
Bolling AFB
Washington, D.C. 20332
Attn: H. Schlossberg — 1 copy

Air Force Weapons Lab
Kirkland AFB
Albuquerque, New Mexico 87117
Attn: Dr. William Baker — 1 copy

Columbia University
520 West 120th Street
Department of Electrical Engineering
New York, N.Y. 10027
Attn: Dr. S.P. Schlesinger — 1 copy

Columbia University
520 West 120th Street
Department of Applied Physics
and Nuclear Engineering
New York, New York 10027
Attn: T.C. Marshall — 1 copy

Cornell University
School of Applied and Engineering Physics
Ithica, New York 14853
Attn: Prof. Hans H. Fleischmann — 1 copy
John Nation — 1 copy
R. N. Sudan — 1 copy

Dartmouth College
18 Wilder, Box 6127
Hanover, New Hampshire 03755
Attn: Dr. John E. Walsh — 1 copy

Department of Energy
Washington, D.C. 20545
Attn: C. Finfgeld/ER-542, GTN — 1 copy
T.V. George/ER-531, GTN — 1 copy
D. Crandall/ER-55, GTN — 1 copy

Defense Advanced Research Project Agency/DEO
1400 Wilson Blvd.
Arlington, Virginia 22209
Attn: Dr. S. Shey — 1 copy
Dr. L. Buchanan — 1 copy

Defense Communications Agency
Washington, D.C. 20305
Attn: Dr. Pravin C. Jain
Assistant for Communications
Technology — 1 copy

Defense Nuclear Agency
Washington, D.C. 20305
Attn: Mr. J. Farber — 1 copy
Maj. J. Benson — 1 copy
Capt. D. Stone — 1 copy
Mr. Lloyd Stossell — 1 copy

Defense Technical Information Center
Cameron Station
5010 Duke Street
Alexandria, Virginia 22314 — 2 copies

Georgia Tech. EES-EOD
Baker Building
Atlanta, Georgia 30332
Attn: Dr. James J. Gallagher — 1 copy

Hanscomb Air Force Base
Stop 21, Massachusetts 01731
Attn: Lt. Rich Nielson/ESD/INK — 1 copy

Hughes Aircraft Co.
Electron Dynamics Division
3100 West Lomita Boulevard
Torrance, California 90509
Attn: J. Christiansen — 1 copy
J.J. Tancredi — 1 copy

KMS Fusion, Inc.
3941 Research Park Dr.
P.O. Box 1567
Ann Arbor, Michigan 48106
Attn: S.B. Segall — 1 copy

Lawrence Livermore National Laboratory
P.O. Box 808
Livermore, California 94550
Attn: Dr. D. Prosnitz — 1 copy
Dr. T.J. Orzechowski — 1 copy
Dr. J. Chase — 1 copy

Los Alamos Scientific Laboratory
P.O. Box 1663, AT5-827
Los Alamos, New Mexico 87545

| | | |
|---|---|---|
| Attn: | Dr. J.C. Goldstein | 1 copy |
| | Dr. T.J.T. Kwan | 1 copy |
| | Dr. L. Thode | 1 copy |
| | Dr. C. Brau | 1 copy |
| | Dr. R. R. Bartsch | 1 copy |

Massachusetts Institute of Technology
Department of Physics
Cambridge, Massachusetts 02139

| | | |
|---|---|---|
| Attn: | Dr. G. Bekefi/36-213 | 1 copy |
| | Dr. M. Porkolab/NW 36-213 | 1 copy |
| | Dr. R. Davidson/NW 16-206 | 1 copy |
| | Dr. A. Bers/NW 38-260 | 1 copy |
| | Dr. K. Kreischer | 1 copy |

Massachusetts Institute of Technology
167 Albany St., N.W. 16-200
Cambridge, Massachusetts 02139

| | | |
|---|---|---|
| Attn: | Dr. R. Temkin/NW 14-4107 | 1 copy |

Spectra Technologies
2755 Northup Way
Bellevue, Washington 98004

| | | |
|---|---|---|
| Attn: | Dr. J.M. Slater | 1 copy |

Mission Research Corporation
Suite 201
5503 Cherokee Avenue
Alexandria, Virginia 22312

| | | |
|---|---|---|
| Attn: | Dr. M. Bollen | 1 copy |
| | Dr. Tom Hargreaves | 1 copy |

Mission Research Corporation
1720 Randolph Road, S.E.
Albuquerque, New Mexico 87106

| | | |
|---|---|---|
| Attn: | Dr. Ken Busby | 1 copy |
| | Mr. Brendan B. Godfrey | 1 copy |

SPAWAR
Washington, D.C. 20363

| | | |
|---|---|---|
| Attn: | E. Warden | |
| | Code PDE 106-3113 | 1 copy |

Naval Research Laboratory

| Addressee: Attn: Name/Code | |
|---|---|
| Code 1001 - T. Coffey | 1 copy |
| Code 1220 - Security | 1 copy |
| Code 2628 - TID Distribution | 22 copies |
| Code 4000 - W. Ellis | 1 copy |
| Code 4600 - D. Nagel | 1 copy |
| Code 4700 - S. Ossakow | 26 copies |

| | |
|---|---|
| Code 4700.1 - A.W. Ali | 1 copy |
| Code 4710 - C. Kapetanakos | 1 copy |
| Code 4740 - Branch Office | 25 copies |
| Code 4740 - W. Black | 1 copy |
| Code 4740 - A. Fliflet | 1 copy |
| Code 4740 - S. Gold | 1 copy |
| Code 4740 - A. Kinkead | 1 copy |
| Code 4740 - W.M. Manheimer | 1 copy |
| Code 4740 - M.E. Read | 1 copy |
| Code 4740 - M. Rhinewine | 1 copy |
| Code 4770 - G. Cooperstein | 1 copy |
| Code 4790 - B. Hui | 1 copy |
| Code 4790 - C.M. Hui | 1 copy |
| Code 4790 - Y.Y. Lau | 1 copy |
| Code 4790 - P. Sprangle | 1 copy |
| Code 5700 - L.A. Cosby | 1 copy |
| Code 6840 - S.Y. Ahn | 1 copy |
| Code 6840 - A. Ganguly | 1 copy |
| Code 6840 - R.K. Parker | 1 copy |
| Code 6840 - N.R. Vanderplaats | 1 copy |
| Code 6850 - L.R. Whicker | 1 copy |
| Code 6875 - R. Wagner | 1 copy |

Naval Sea Systems Command
Department of the Navy
Washington, D.C. 20362
Attn: Commander George Bates
PMS 405-300 — 1 copy

Northrop Corporation
Defense Systems Division
600 Hicks Rd.
Rolling Meadows, Illinois 60008
Attn: Dr. Gunter Dohler — 1 copy

Oak Ridge National Laboratory
P.O. Box Y
Mail Stop 3
Building 9201-2
Oak Ridge, Tennessee 37830
Attn: Dr. A. England — 1 copy

Office of Naval Research
800 N. Quincy Street
Arlington, Va. 22217
Attn: Dr. C. Roberson — 1 copy
Dr. W. Condell — 1 copy
Dr. T. Berlincourt — 1 copy

Office of Naval Research
1030 E. Green Street
Pasadena, CA 91106
Attn: Dr. R. Behringer — 1 copy

University of Tennessee
Dept. of Electrical Engr.
Knoxville, Tennessee 37916
Attn: Dr. I. Alexeff — 1 copy

University of New Mexico
Department of Physics and Astronomy
800 Yale Blvd, N.E.
Albuquerque, New Mexico 87131
Attn: Dr. Gerald T. Moore — 1 copy

University of Utah
Deparment of Electrical Engineering
3053 Merrill Engineering Bldg.
Salt Lake City, Utah 84112
Attn: Dr. Larry Barnett — 1 copy
Dr. J. Mark Baird — 1 copy

U. S. Naval Academy
Annapolis, Maryland 21402-5021 — 1 copy

U. S. Army
Harry Diamond Labs
2800 Powder Mill Road
Adelphi, Maryland 20783-1145
Attn: Dr. Edward Brown — 1 copy
Dr. Michael Chaffey — 1 copy

Varian Associates
611 Hansen Way
Palo Alto, California 94303
Attn: Dr. H. Jory — 1 copy
Dr. David Stone — 1 copy
Dr. Kevin Felch — 1 copy
Dr. A. Salop — 1 copy

Varian Eimac San Carlos Division
301 Industrial Way
San Carlos, California 94070
Attn: C. Marshall Loring — 1 copy

Yale University
Applied Physics
Madison Lab
P.O. Box 2159
Yale Station
New Haven, Connecticut 06520
Attn: Dr. N. Ebrahim — 1 copy
Dr. I. Bernstein — 1 copy

Director of Research
U.S. Naval Academy
Annapolis, Maryland 21402 — 2 copies

NRL Code 1220 — 1 copy

Records — 1 copy

Science Applications, Inc.
1710 Goodridge Dr.
McLean, Virginia 22102
Attn: Adam Drobot — 1 copy
P. Vitrello — 1 copy

Stanford University
High Energy Physics Laboratory
Stanford, California 94305
Attn: Dr. T.I. Smith — 1 copy

TRW, Inc.
Space and Technology Group
Suite 2600
1000 Wilson Boulevard
Arlington, VA 22209
Attn: Dr. Neil C. Schoen — 1 copy

TRW, Inc.
Redondo Beach, California 90278
Attn: Dr. H. Boehmer — 1 copy
Dr. T. Romisser — 1 copy

University of California
Physics Department
Irvine, California 92717
Attn: Dr. G. Benford — 1 copy
Dr. N. Rostoker — 1 copy

University of California
Department of Physics
Los Angeles, CA 90024
Attn: Dr. A.T. Lin — 1 copy
Dr. N. Luhmann — 1 copy
Dr. D. McDermott — 1 copy

University of Maryland
Department of Electrical Engineering
College Park, Maryland 20742
Attn: Dr. V. L. Granatstein — 1 copy
Dr. W. W. Destler — 1 copy

University of Maryland
Laboratory for Plasma and Fusion
Energy Studies
College Park, Maryland 20742
Attn: Dr. Jhan Varyan Hellman — 1 copy
Dr. John McAdoo — 1 copy
Dr. John Finn — 1 copy
Dr. Baruch Levush — 1 copy
Dr. Tom Antonsen — 1 copy
Dr. Edward Ott — 1 copy

Optical Sciences Center
University of Arizona
Tucson, Arizona 85721
Attn: Dr. Willis E. Lamb, Jr. — 1 copy

OSD/SDIO
Attn: IST (Dr. H. Brandt)
Washington, D.C. 20301-7100 — 1 copy

Pacific Missile Test Center
Code 0141-5
Point Muga, California 93042
Attn: Will E. Chandler — 1 copy

Physical Dynamics, Inc.
P.O. Box 10367
Oakland, California 94610
Attn: A. Thomson — 1 copy

Physics International
2700 Merced Street
San Leandro, California 94577
Attn: Dr. J. Benford — 1 copy

Princeton Plasma
Plasma Physics Laboratory
James Forrestal Campus
P.O. Box 451
Princeton, New Jersey 08544
Attn: Dr. H. Hsuan — 2 copies
Dr. J. Doane — 1 copy

Quantum Institute
University of California
Santa Barbara, California 93106
Attn: Dr. L. Elias — 1 copy

Raytheon Company
Microwave Power Tube Division
Foundry Avenue
Waltham, Massachusetts 02154
Attn: N. Dionne — 1 copy

Sandia National Laboratories
ORG. 1231, P.O. Box 5800
Albuquerque, New Mexico 87185
Attn: Dr. Thomas P. Wright — 1 copy
Mr. J.E. Powell — 1 copy
Dr. J. Hoffman — 1 copy
Dr. W.P. Ballard — 1 copy
Dr. C. Clark — 1 copy

END

11-87

DTIC